# STELLAR EVOLUTION. VI. EVOLUTION FROM THE MAIN SEQUENCE TO THE RED-GIANT BRANCH FOR STARS OF MASS 1 $M_\odot$, 1.25 $M_\odot$, AND 1.5 $M_\odot$*

ICKO IBEN, JR.
Massachusetts Institute of Technology
*Received May 31, 1966*

## ABSTRACT

Evolution from the main sequence to the red-giant phase is discussed for Population I stars of mass $M/M_\odot = 1$, 1.25, and 1 5. Prior to the giant phase in all three stars, energy generation by the $p$-$p$ chain reactions dominates over energy generation by the CN cycle reactions. During the main hydrogen-burning phase, a convective core is not present in the 1 $M_\odot$ star but does occur in both the 1.25 $M_\odot$ and 1.5 $M_\odot$ stars. Over a major portion of the main-sequence phase, the convective core *grows* in both the 1.25 $M_\odot$ and 1.5 $M_\odot$ stars as the CN cycle reactions become increasingly important. As each star rises along the red-giant branch, the CN cycle reactions eventually become the major source of energy in the hydrogen-burning shell.

The time spent by a star burning hydrogen in a thick shell relative to the time spent in the core hydrogen-burning phase is found to be a strongly decreasing function of stellar mass. Partially responsible for this mass dependence are three factors: (1) for more massive stars, the mass fraction in the convective core, and hence the mass over which hydrogen is exhausted at the end of the core hydrogen-burning phase, is closer to the effective Schönberg-Chandrasekhar limit; (2) with decreasing stellar mass, the variation of hydrogen through the shell becomes more gradual, and (3) with decreasing mass, electron degeneracy becomes more important in the hydrogen-exhausted core during the thick shell-burning phase. The latter two factors have the effect of increasing the Schönberg-Chandrasekhar limit.

In contrast with the case of more massive stars discussed in earlier papers of this series, electron degeneracy is responsible for a major fraction of the pressure and electron conduction is the major mode of energy flow in the hydrogen-exhausted core of all three stars during the giant phase The result is that all three stars possess a nearly isothermal core along the giant branch.

During and following the shell-narrowing phase in all three stars, the surface lithium abundance decreases regularly with decreasing surface temperature as envelope convection extends deeper and deeper into the star. Such is the case also for the surface ratio of $C^{12}$ to $N^{14}$. Comparatively large amounts of $He^3$ are made in all three stars, and it is suggested that a large fraction of the $He^3$ in the galactic disk was perhaps formed in ordinary stars.

Comparison of individual tracks with cluster diagrams for NGC 188 and M67 provides evidence for the qualitative correctness of several characteristic features of the theoretical tracks. The pronounced and rapid change in luminosity and in surface temperature during the phase of over-all contraction is related to a "gap" in M67; the decrease with decreasing mass in the magnitude of the luminosity drop during the shell-narrowing phase is related to the change with cluster age in the slope of the subgiant branch; for a given luminosity, the decrease with decreasing mass in surface temperature along the giant branch is related to the decrease with increasing cluster age in surface temperature along the cluster giant branch. The ages of NGC 188 and M67 are estimated to be $(11 \pm 2) \times 10^9$ yr and $(5.5 \pm 1) \times 10^9$ yr, respectively.

## I. INTRODUCTION

It has been demonstrated (see, e.g., Hofmeister, Kippenhahn, and Weigert 1964) that, by means of relaxation techniques, the evolution of fairly massive stars may be followed quite readily from the main sequence through the core helium-burning phase. By use of these same techniques, low-mass stars may be readily followed to the early-giant phase preceding the helium flash. However, the occurrence of strong electron degeneracy in the hydrogen-exhausted core of low-mass giants leads to a relatively extended period of pure hydrogen burning in an extremely thin shell. The minuteness of the shell forces the use of very small time steps and thereby necessitates the expenditure of very large amounts of computation time. For this reason, the evolution of low-mass stars described in this paper has been terminated along the giant branch.

* Supported in part by the National Aeronautics and Space Administration (NSG-496).

The equations, constitutive relations, and methods of solution employed in constructing the models presented here are identical with those described in Papers I–V (Iben 1965*a*, *b*; 1966*a*, *b*, *c*).

In § II, comparisons are drawn between the time-dependent characteristics of models of mass 1 $M_\odot$, 1.25 $M_\odot$, and 1.5 $M_\odot$. Structural characteristics of a few selected models are described in § III, § IV, and § V. Finally, observational consequences are sketched in § VI.

## II. TIME-DEPENDENT CHARACTERISTICS

Evolutionary tracks in the H-R diagram for stars of mass 1 $M_\odot$, 1.25 $M_\odot$, and 1.5 $M_\odot$ are shown in Figure 1. Times to reach circled points along the tracks are given in Table 1 in units of $10^9$ yr.

Several distinguishing features are immediately apparent. (1) As stellar mass is decreased, the direction of early evolution off the main sequence gradually shifts from movement to the red to movement to the blue. (2) The phase of over-all contraction and increasing surface temperature (points 3 to 4) following the major hydrogen-burning phase (points 1 to 3) becomes less pronounced with decreasing mass, disappearing be-

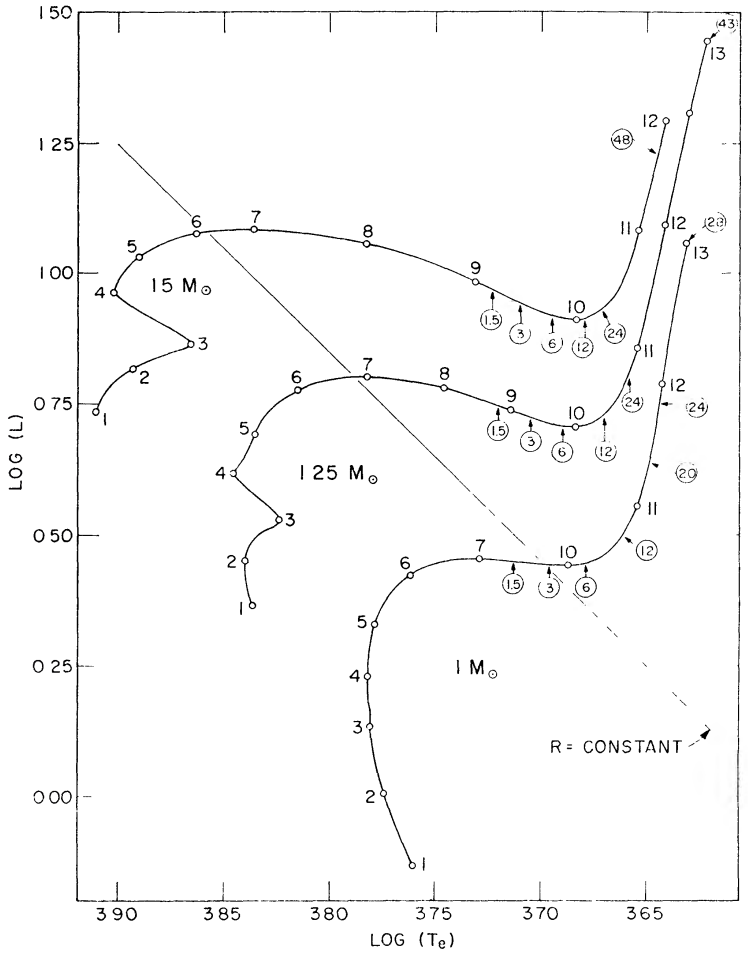


FIG. 1.—Evolutionary paths for Population I stars of mass $M/M_\odot$ = 1, 1.25, and 1 5. Times to reach labeled points along each track are given in Table 1. Luminosity $L$ is in solar units and surface temperature $T_e$ is in degrees Kelvin Circled numbers represent the factors by which surface $Li^7$ abundance has been depleted relative to its main sequence value The straight line is one of constant radius $R$

tween 1.25 $M\odot$ and 1 $M\odot$. This is as one might expect, since core convection during the major hydrogen-burning phase vanishes in this mass range. (3) During the shell narrowing phase (points 7 to 10), the drop in luminosity decreases with decreasing mass. This drop amounts to $-\Delta(\log L) = 0.15$, 0.10, and 0.015 for masses 1.5 $M\odot$, 1.25 $M\odot$, and 1 $M\odot$, respectively. (4) The increase in luminosity between points 1 and 7 diminishes with increasing mass, amounting to $\Delta(\log L) = 0.69$, 0.44, and 0.35 for masses 1 $M\odot$, 1.25 $M\odot$, and 1.5 $M\odot$, respectively.

It is to be emphasized that, for all masses, stellar radius increases throughout the major core hydrogen-burning phase. To illustrate this fact, a line of constant radius has been drawn in Figure 1.

The time dependence of selected observable and interior characteristics is shown in Figures 2 and 3 (1 $M\odot$), Figures 4 and 5 (1.25 $M\odot$), and Figures 6 and 7 (1.5 $M\odot$). A comparison of quantities in these figures is instructive.

During the first portion of the main-sequence or core hydrogen-burning phase of all three stars, energy generation by the *p-p* chains dominates over energy production by

TABLE 1

EVOLUTIONARY LIFETIMES ($10^9$ yr)

| Point | 1 $M\odot$ | 1 25 $M\odot$ | 1 50 $M\odot$ |
|---|---|---|---|
| 1 | 0 05060 | 0 02954 | 0 01821 |
| 2 | 3 8209 | 1 4220 | 1 0277 |
| 3 | 6 7100 | 2 8320 | 1 5710 |
| 4 | 8 1719 | 3 0144 | 1 6520 |
| 5 | 9 2012 | 3 5524 | 1 8261 |
| 6 | 9 9030 | 3 9213 | 1 9666 |
| 7 | 10 195 | 4 0597 | 2 0010 |
| 8 | | 4 1204 | 2 0397 |
| 9 | .. ... | 4 1593 | 2 0676 |
| 10 | 10 352 | 4 2060 | 2 1059 |
| 11 | 10 565 | 4 3427 | 2 1991 |
| 12 | 10 750 | 4 4505 | 2 2628 |
| 13 | 10 875 | 4 5349 | |

the CN cycle. This dominance increases with decreasing mass until, between 1 $M\odot$ and 1.25 $M\odot$, core convection during the core hydrogen-burning phase disappears. When a convective core does occur in the star, however, as in the 1.25 $M\odot$ and 1.5 $M\odot$ cases, core mass *increases* initially with time as the CN cycle reactions increase in relative importance.

In contradistinction with the more massive stars studied in earlier papers of this series, central temperatures and densities rise *throughout* the main-sequence phase; the decreased rate at which $O^{16}$ is converted into $N^{14}$ in the stellar core is responsible for this. Note that by the end of the core hydrogen-burning phase of the 1 $M\odot$ star, $t \sim 7 \times 10^9$ yr, $O^{16}$ at the stellar center is reduced by only a factor of 3 from its initial main-sequence value. It is reduced by factors of approximately 5 and 10 in stars of mass 1.25 $M\odot$ and 1.5 $M\odot$, respectively.

The phase of over-all contraction following the major core hydrogen-burning phase is quite pronounced for the 1.25 $M\odot$ and 1.5 $M\odot$ stars but does not occur in 1 $M\odot$ evolution. The reason for this is, of course, the fact that hydrogen is reduced uniformly over a relatively large fraction of the nuclear-burning region in the more massive stars, whereas hydrogen decreases gradually toward the center through the nuclear-burning region of the 1 $M\odot$ star. As hydrogen is reduced rapidly over relatively large regions in the more massive stars, rapid contraction and heating are necessary to maintain core nuclear burning at a sufficiently high level. This is not the case for the 1 $M\odot$ star.

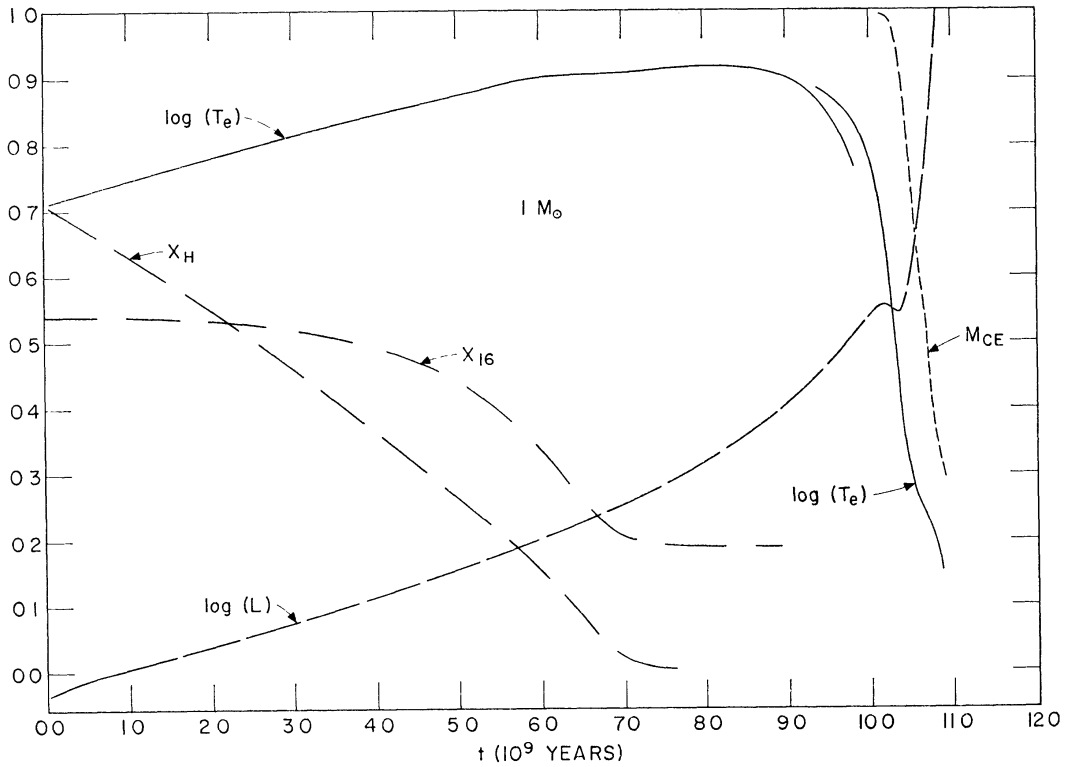


FIG 2 —The variation with time, for a 1 $M\odot$ star, of luminosity ($L$), surface temperature ($T_e$), mass fraction outside of which energy flows by convection ($M_{CE}$), and central abundance by mass of $H^1(X_H)$ and $O^{16}(X_{16})$ Time ($t$) in this figure and in Figs 3–7 is measured in units of $10^9$ yr. The unit of luminosity is $L\odot = 3\ 86 \times 10^{33}$ ergs/sec and the unit of surface temperature is degrees Kelvin Scale limits (0 0–1.0 on the vertical scale) correspond to $-0\ 1 \leq \log L \leq 0.9$, $3\ 69 \leq \log T_e \leq 3.79$ (up to $t \sim 9\ 8$), $3.60 \leq \log T_e \leq 3\ 80$ (beyond $t \sim 9\ 38$), $0\ 0 < M_{CE} < 1\ 0$, $0\ 0 \leq X_H \leq 1.0$, and $0\ 0 \leq X_{16} \leq 0\ 02$.

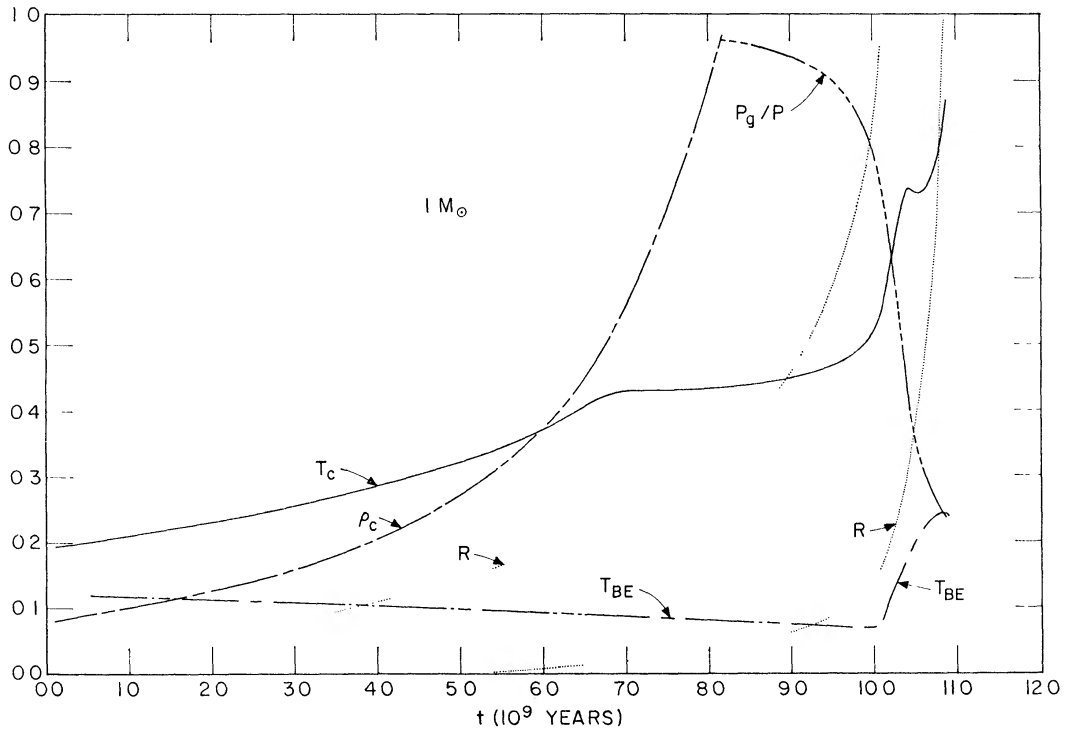


FIG. 3 —The variation with time, for a 1 $M\odot$ star, of radius ($R$), central density ($\rho_c$), central temperature ($T_c$), temperature at the base of the convective envelope ($T_{BE}$), and the central ratio of gas pressure computed via the perfect gas equation of state, $P_g$, to the total gas pressure, $P$. Units are $R\odot = 6\ 96 \times 10^{10}$ cm for radius, $10^{6\circ}$ K for temperature, and grams per cubic centimeter for density. Scale limits correspond to $0\ 85 \leq R \leq 1.85$ ($t \lesssim 10\ 1$), $1.0 \leq R \leq 6\ 0$ ($t \gtrsim 5.4$), $50 \leq \rho_c \leq 550$, $10 \leq T_c \leq 30$, $0.0 \leq P_g/P \leq 1\ 0$, and $0.0 \leq T_{BE} \leq 10\ 0$.

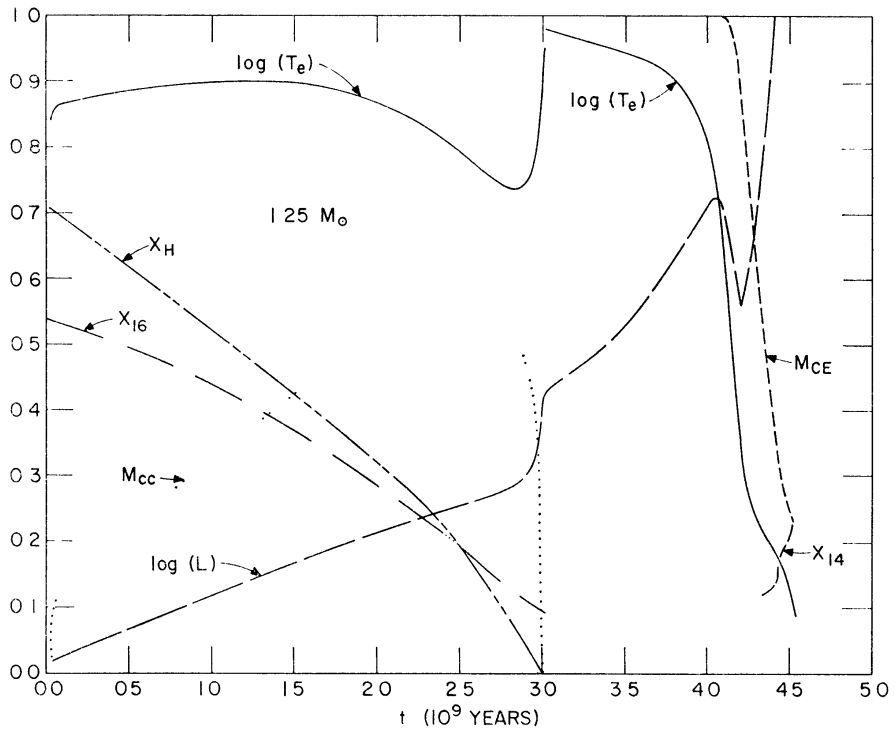


FIG. 4.—The variation with time of characteristics describing a 1.25 $M\odot$ star. Variables and units are the same as in Figs. 2 and 3. In addition, $M_{cc}$ = mass fraction in the convective core and $X_{14}$ = *surface* abundance by mass of $N^{14}$. Scale limits correspond to $0.35 \leq \log L \leq 0.975$, $3\,75 \leq \log T_e \leq 3\,85$ ($t \lesssim 3$), $3.60 \leq \log T_e \leq 3\,85$ ($t \gtrsim 3$), $0.0 \leq M_{CE} \leq 1\,0$, $0.0 \leq M_{cc} \leq 0\,08$, $0.0 \leq X_H \leq 1.0$, $0\,0 \leq X_{16} \leq 0\,02$, and $0\,0 \leq X_{14} \leq 0\,01$.

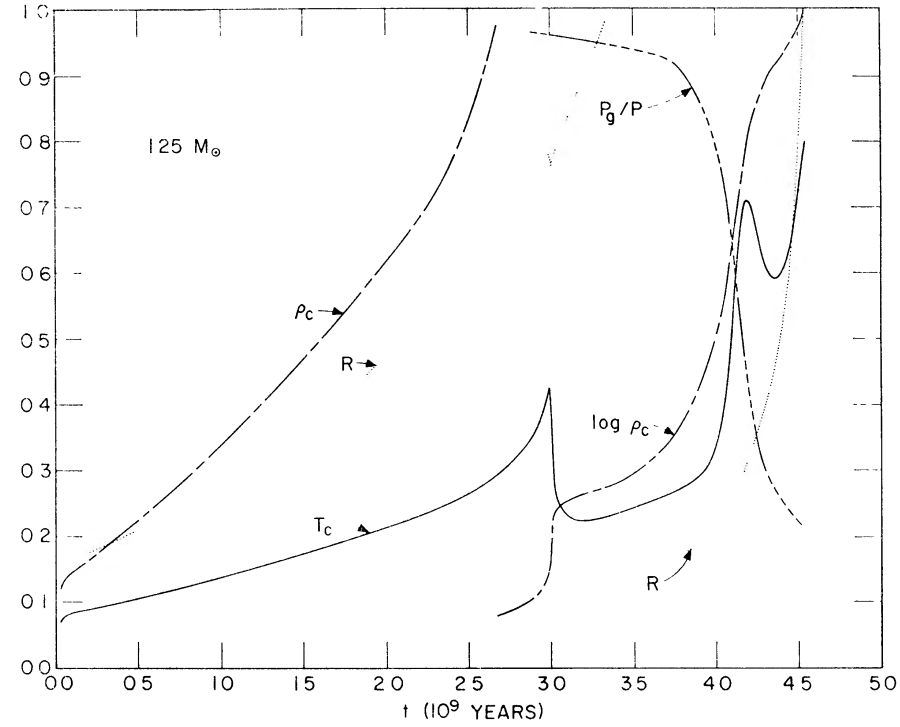


FIG. 5.—The variation with time, for a 1.25 $M\odot$ star, of the same variables shown in previous figures. Units are the same as in Figs. 2 and 3. Scale limits correspond to $1.0 \leq R \leq 1.5$ ($t \lesssim 3.32$), $0 \leq R \leq 10$ ($t \gtrsim 3\,16$), $15 \leq T_c \leq 35$, $80 \leq \rho_c \leq 180$, $2.0 \leq \log \rho_c \leq 5.125$, and $0.0 \leq P_g/P \leq 1.0$.

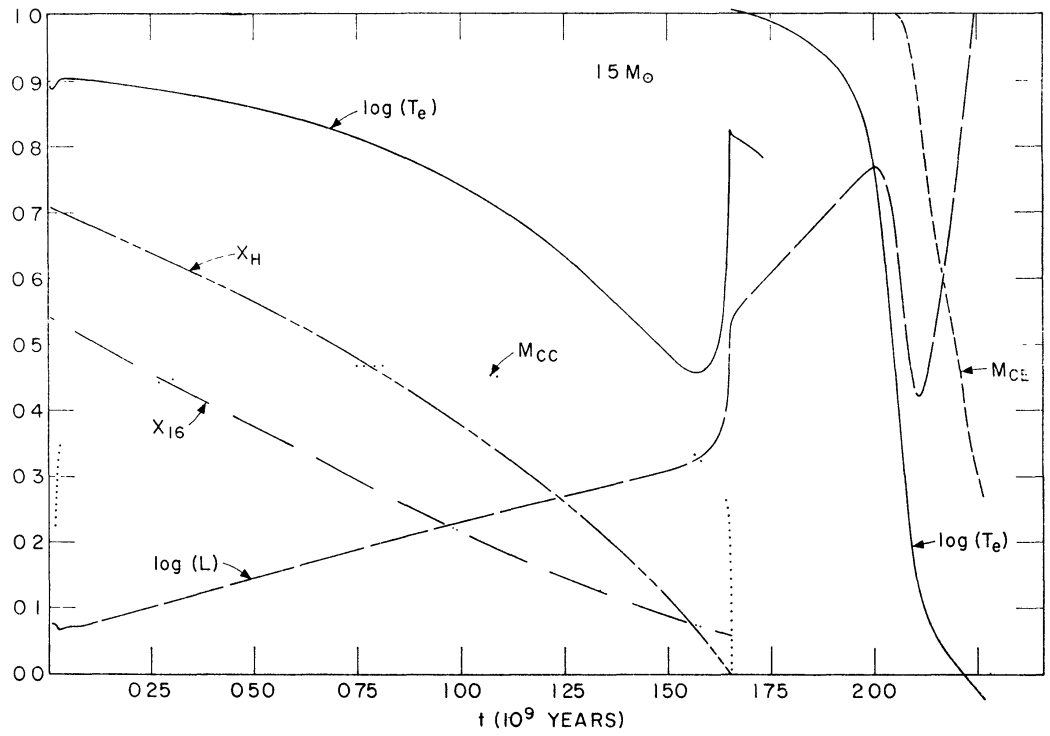


FIG. 6.—The variation with time, for a 1 5 $M\odot$ star, of the same variables shown in previous figures. Units are the same as in these figures Scale limits correspond to 0 7 $\leq \log L \leq 1.2$, 3.82 $\leq \log T_e \leq$ 3.92 ($t \lesssim 1.74$), 3.65 $\leq \log T_e \leq 3.90$ ($t > 1.65$), 0 0 $\leq M_{CE} \leq 1.0$, 0.0 $\leq M_{cc} \leq 1/6$, 0.0 $\leq X_H \leq$ 1.0, and 0 0 $\leq X_{16} \leq 0.02$.

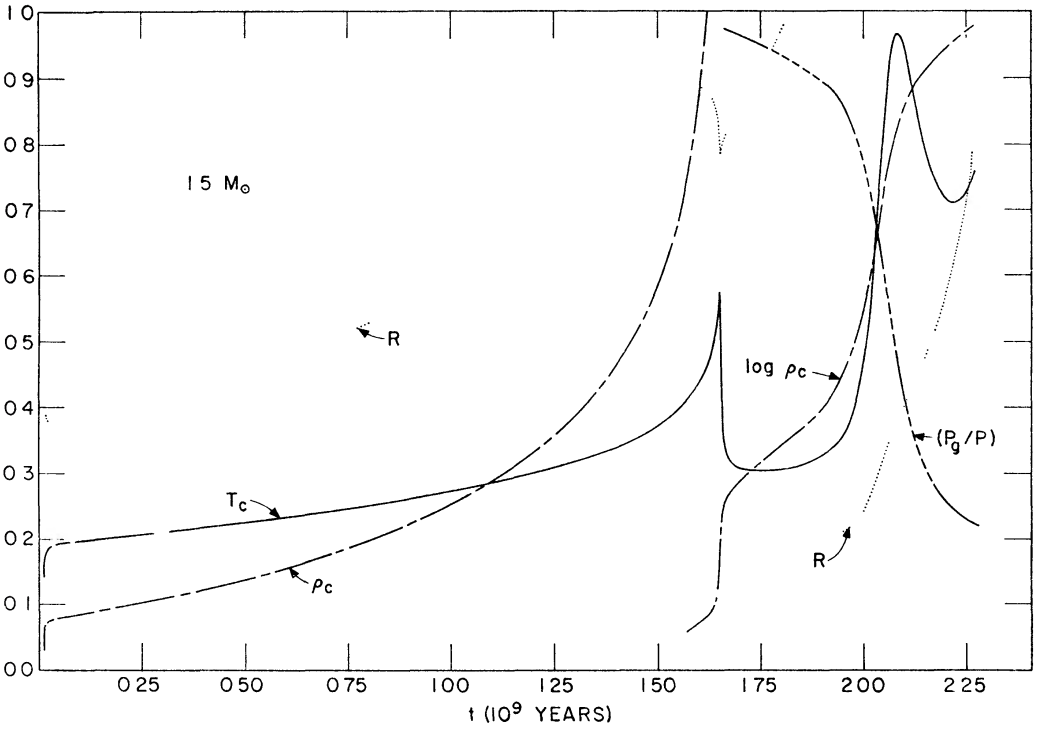


FIG. 7.—The variation with time, for a 1.5 $M\odot$ star of the same variables shown in previous figures. Units are the same as in these figures. Scale limits correspond to 0 8 $\leq R \leq 1.8$ ($t \lesssim 1$ 8), 0 $\leq R \leq 10$ ($t \gtrsim 1$ 68), 15 $\leq T_c \leq 35$, 80 $\leq \rho_c \leq 180$, 2.0 $\leq \log \rho_c \leq 5$ 125, and 0 0 $\leq P_g/P \leq 1.0$.

The rapid central cooling and condensation which mark the shell-development stage near points 4 in the 1.25 $M_\odot$ and 1.5 $M_\odot$ cases are absent in the 1 $M_\odot$ case, the reason again being the absence of a convective core during the main-sequence phase of 1 $M_\odot$ evolution. Since, in the 1 $M_\odot$ case, the core hydrogen-burning phase merges smoothly with the phase of hydrogen burning in a thick shell, one cannot make the clear-cut distinction between the two phases that is possible for the more massive stars. In earlier papers it was demonstrated that the time spent by a star burning hydrogen in a thick shell, $\tau_{\text{shell}}$, relative to the lifetime for core hydrogen burning, $\tau_{\text{MS}}$, is a decreasing function of mass. For example, $\tau_{\text{shell}}/\tau_{\text{MS}} = 0.0204$ and 0.0461 for stars of mass 5 $M_\odot$ and 3 $M_\odot$, respectively. Defining the thick shell-burning phase for the 1.25 $M_\odot$ and 1.5 $M_\odot$ stars as the interval between points 4 and 7 in Figure 1, one finds $\tau_{\text{shell}}/\tau_{\text{MS}} = 0.225$ in the 1.5 $M_\odot$ case and $\tau_{\text{shell}}/\tau_{\text{MS}} = 0.372$ in the 1.25 $M_\odot$ case. The increase in $\tau_{\text{shell}}/\tau_{\text{MS}}$ with decreasing mass is related to the magnitude of the convective core during the main-sequence phase. The closer the mass fraction of the convective core is to the effective Schönberg-Chandrasekhar (1942) limit, the smaller is the mass fraction through which the thick shell may move before the shell narrows and the star adopts a giant structure.

The drop in luminosity between points 7 and 10 along all tracks in Figure 1 is a feature held in common with more massive stars. The drop is brought about by a reduction in strength of the rapidly narrowing hydrogen-burning shell and by simultaneous absorption in the rapidly expanding (primarily radiative) stellar envelope. The increase in luminosity beyond points 10 occurs when photospheric layers, outside of a growing convective envelope that neither absorbs energy from the interior nor responds sensitively to changes in envelope opacity, begin to significantly influence energy production in the shell. The decrease with mass in the magnitude of the luminosity drop during the shell-narrowing phase is related to the fact that, in the mass range considered here, the relative control of surface layers, within which opacity (primarily due to $H^-$ absorption) decreases with decreasing temperature, is essentially a function only of surface temperature (i.e., of the surface energy flux), nearly independent of stellar mass. Therefore, the surface demand for increasing luminosity is satisfied at approximately the same surface temperature for all stars. When this fact is coupled with the fact that the surface temperature at the start of the shell-narrowing phase (points 7) is closer to the surface temperature at the start of the giant phase (points 10) for smaller stellar masses, it becomes understandable that the luminosity drop during the shell-narrowing phase becomes less pronounced with decreasing stellar mass.

The hydrogen-burning shell continues to decrease in thickness as the stars move beyond points 10 in Figure 1. Core temperatures and densities continue to rise rapidly until electron degeneracy begins to assume a dominant role in supplying core pressure. In all three stars, central temperature drops when the additional contribution to the pressure due to electron degeneracy exceeds the pressure due to electron thermal motions by a factor of approximately 2. This is demonstrated by the curves $T_c$ and $P_g/P$ versus time in Figures 3, 5, and 7. $P$ denotes the total central pressure and $P_g$ denotes the central pressure which would occur if pressure were supplied solely by thermal motions of electrons and positive ions.

During the period of hydrogen burning in a thick shell, the hydrogen-exhausted core is nearly isothermal in all three stars. During the shell-narrowing stage, a large temperature gradient is built up between the center and the shell. The required heat is supplied by the release of gravitational energy, and the energy release necessary to maintain the temperature gradient is also supplied by the release of gravitational energy. As the core becomes more degenerate, the rate of core condensation decreases and electron conduction becomes more effective. The net result is a second approach to isothermal conditions in the hydrogen-exhausted core; the central temperature continues to drop until it approaches shell temperatures. As the core continues to contract and luminosity

continues to rise, shell and therefore core temperatures again rise together until central temperatures become high enough to ignite the $N^{14}$ $(\alpha,\gamma)F^{18}$ $(\beta^+\nu)O^{18}$ reactions.

## III. STRUCTURAL DETAILS DURING 1 $M_\odot$ EVOLUTION

The variation of physical variables in the 1 $M_\odot$ star as it reaches the main sequence may be found in Paper I.

In Figure 8 are exhibited state and composition variables when the 1 $M_\odot$ star is slightly younger than the Sun, $t = 4.27 \times 10^9$ yr. Three features distinguish the star at

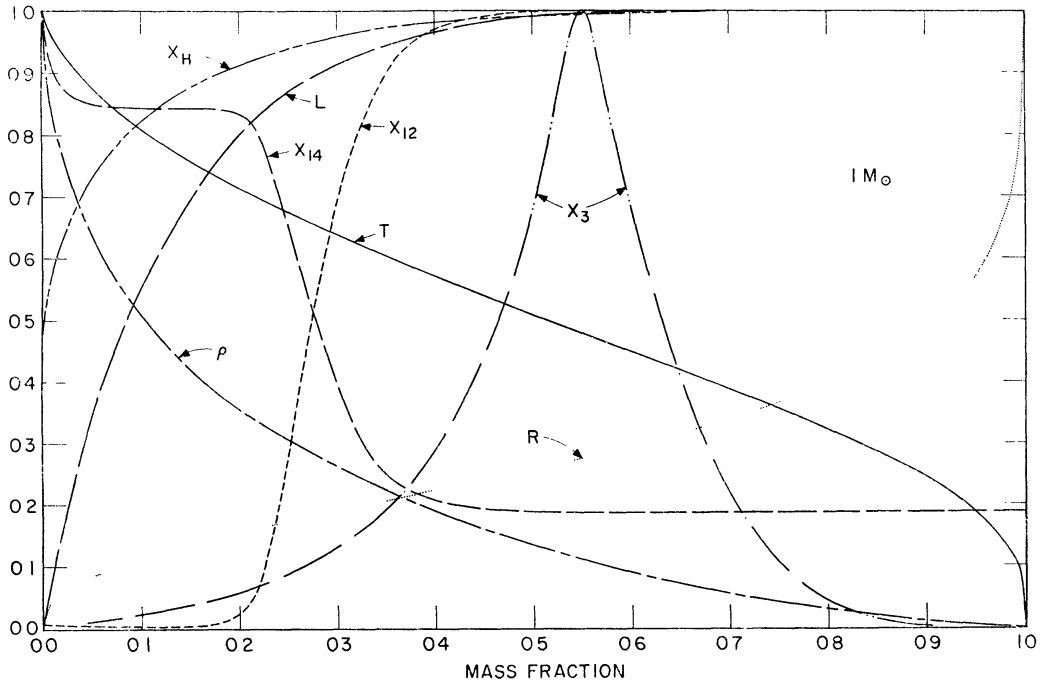


FIG 8.—The variation with mass fraction, for a 1 $M_\odot$ star, of state and composition variables when $t = 4.26990 \times 10^9$ yr. Variables have the significance: $\rho$ = density (gm/cm$^3$), $T$ = temperature ($10^6$ ° K), $L$ = luminosity ($3\,86 \times 10^{33}$ ergs/sec), $R$ = radius ($6\,96 \times 10^{10}$ cm), and $X_i$ = central abundance by mass of $H^1(X_H)$, $He^3(X_3)$, $C^{12}(X_{12})$, and $N^{14}(X_{14})$ Scale limits correspond to $0\,0 \leq \rho \leq 159\,93$, $0.0 \leq T \leq 15.910$, $0.0 \leq L \leq 1.0575$, $0.0 \leq R \leq 0.96830$, $0.0 \leq X_H \leq 0\,708$, $0\,0 \leq X_3 \leq 4\,20 \times 10^{-3}$, $0.0 \leq X_{12} \leq 3.61 \times 10^{-3}$, and $0\,0 \leq X_{14} \leq 6\,40 \times 10^{-3}$ The mass fraction in the static envelope is $9\,9622 \times 10^{-5}$, as it is also in Figs 9–11, and stellar radius is $R_s = 0\,96830\ R_\odot$. Central pressure (not shown) is $2\,5186 \times 10^{17}$ dyne/cm$^2$.

this time from more massive stars at comparable stages of development. The most obvious feature is the lack of a convective core. Second, energy sources are spread out over a much larger mass fraction than is the case with stars burning primarily via the CN cycle. This is, of course, due to the less steep temperature dependence of the *p-p* chain reaction rates. Third, $O^{16}$ has only begun to be converted into $N^{14}$ near the very center of the star and $C^{12}$ is still being converted into $N^{14}$ within the region of significant energy generation.

It is of interest to note that considerable $He^3$ is built up in the 1 $M_\odot$ star far from the major region of energy production. The abundance by mass of $He^3$ reaches a maximum of $(X_3)_{max} \sim 4.2 \times 10^{-3}$ at a mass fraction of 0.553. This is approximately ten times larger than the maximum achieved in the interior of the 3 $M_\odot$ star described in Paper II. The $C^{12}$ transition layer (where one-half of the original $C^{12}$ has been converted into $N^{14}$) occurs at a mass fraction of 0.275.

A convective envelope extends over the outer 0.0186 $M_\odot$ of the star. At the base of the envelope, temperature and density reach the values $T_{BE} = 10^6$ ° K and $\rho_{BE} = 0.023$ gm/cm$^3$, respectively. During the entire period of core hydrogen burning, the temperature at the base of the convective envelope remains below $1.2 \times 10^6$ ° K (see curve $T_{BE}$ versus $t$ in Fig. 2) so that, in the envelope, a light element such as lithium does not undergo thermonuclear disintegration to any significant degree after the star reaches the main sequence.

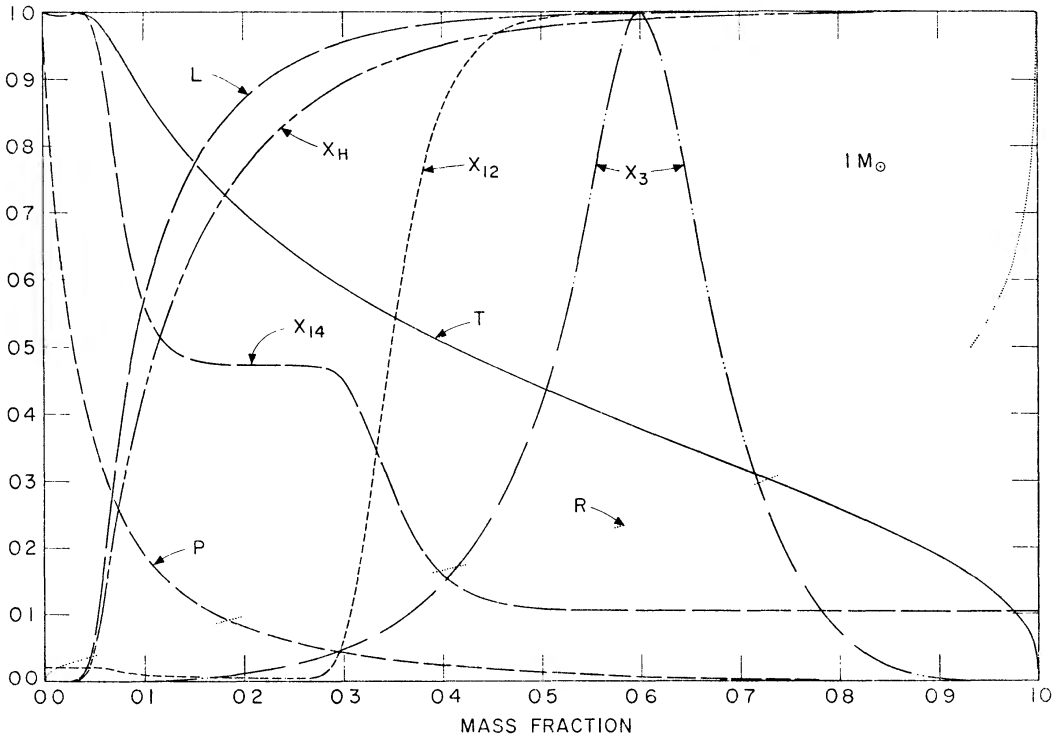


FIG 9.—The variation with mass fraction, for a 1 $M_\odot$ star, of state and composition variables when $t = 9.20150 \times 10^9$ yr. Variables have the same significance and units as in Fig. 8 In addition, pressure $P$ is given in units of $10^{17}$ dyne/cm$^2$. Scale limits correspond to $0\,0 \leq P \leq 13\,146$, $0\,0 \leq T \leq 19.097$, $0\,0 \leq L \leq 2.1283$, $0.0 \leq R \leq 1.2681$, $0\,0 \leq X_H \leq 0\,708$, $0.0 \leq X_3 \leq 5.15 \times 10^{-3}$, $0.0 \leq X_{12} \leq 3\,61 \times 10^{-3}$, and $0.0 \leq X_{14} \leq 1.15 \times 10^{-2}$. Stellar radius is $R_s = 1\,3526\ R_\odot$, and central density (not shown) is 1026 0 gm/cm$^3$.

Hydrogen may be considered to be effectively exhausted at the stellar center when the rate of energy release from the gravitational field and from thermal motions ($\epsilon_{grav}$) becomes comparable with the rate of nuclear energy production ($\epsilon_{nuc}$) at the center. This occurs in the 1 $M_\odot$ star at $t = 8.44 \times 10^9$ yr when hydrogen at the center reaches $X_H \sim 10^{-5}$. In contrast with more massive stars, central temperature does not drop significantly as the growing hydrogen-exhausted core becomes isothermal. Instead, temperatures at the base of the hydrogen-burning shell rise to reach the core temperature.

Conditions within the star at $t = 9.20 \times 10^9$ yr, when the isothermal core extends over approximately the inner 4 per cent of the star's mass, are shown in Figure 9. In comparison with more massive stars during the period of thick shell burning, the region of energy production extends over a very wide region. The shell "center," defined as the point at which the luminosity variable is one-half the surface luminosity, is at a mass fraction ~0.09. Eighty per cent of the total escaping energy is contributed by the region between mass fractions 0.053 and 0.225. Thus, during the period of thick shell burning

in the 1 $M_\odot$ star, the relative thickness of the hydrogen-burning shell is $\Delta M_{\text{shell}}/M_{\text{star}} = 0.172$, a value which is approximately three times greater than in stars of mass $M \geq 3\ M_\odot$.

In the isothermal core, 65 per cent of the original $O^{16}$ has been converted into $N^{14}$. The maximum abundance of $He^3$, $(X_3)_{\max} = 5.15 \times 10^{-3}$, occurs at a mass fraction 0.597 and the $C^{12}$ transition layer has moved out to a mass fraction 0.35. $Li^7$ has been depleted over approximately the inner 97.5 per cent of the star's mass.

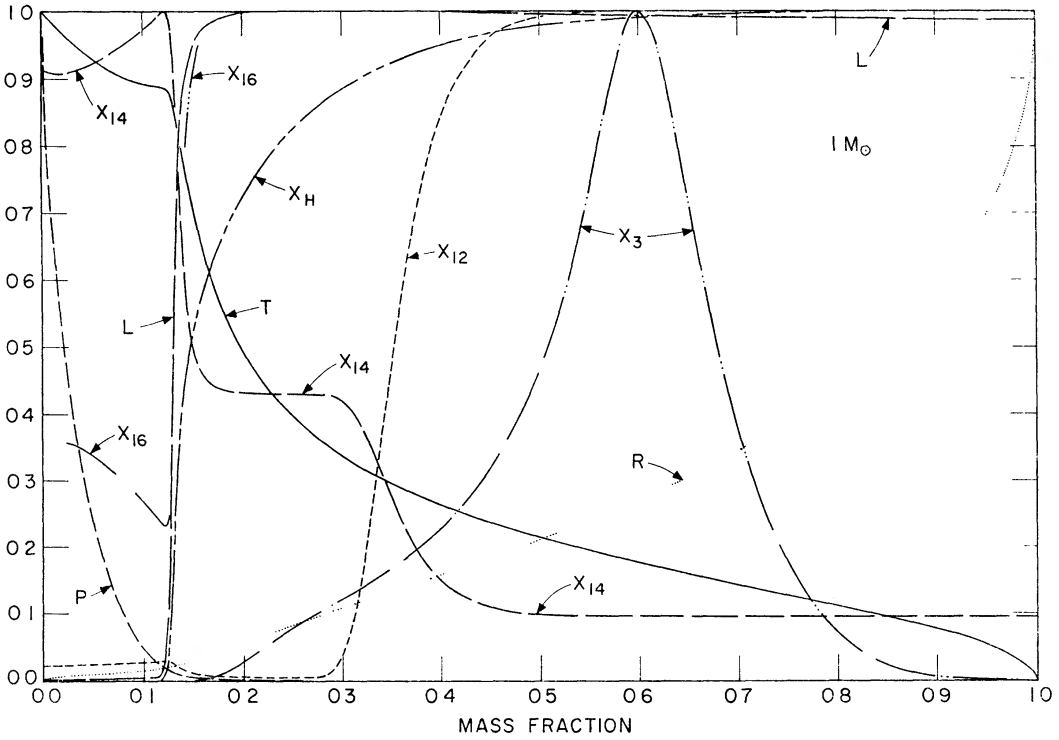


FIG. 10.—The variation with mass fraction, for a 1 $M_\odot$ star, of state and composition variables when $t = 10\ 3059 \times 10^9$ yr Variables have the same significance and units as in Figs 8 and 9 In addition $X_{16}$ = central abundance by mass of $O^{16}$. Scale limits correspond to $0\ 0 \leq P \leq 415.15$, $0\ 0 \leq T \leq 23.868$, $0\ 0 \leq L \leq 2\ 8227$, $0\ 0 \leq R \leq 2.1334$, $0\ 0 \leq X_{\text{H}} \leq 0\ 708$, $0\ 0 \leq X_3 \leq 5.35 \times 10^{-3}$, $0\ 0 \leq X_{12} \leq 3.61 \times 10^{-3}$, $0\ 0 \leq X_{14} \leq 1\ 26 \times 10^{-2}$, and $0\ 0 \leq X_{16} \leq 1\ 08 \times 10^{-2}$. Stellar radius is $R_s = 2.2179\ R_\odot$, and central density (not shown) is 15214 gm/cm³.

Pressure in the isothermal core is not due entirely to thermal motions. At the center, where the density is $\rho_c = 1.026 \times 10^3$ gm/cm³ and temperature is $T_c = 19.097 \times 10^6$ ° K, electron degeneracy leads to a 7.5 per cent contribution to the total pressure. The appropriate Schönberg-Chandrasekhar (1942) limit will therefore be somewhat larger than would be the case if degeneracy had been neglected.

When the mass in the hydrogen-exhausted core begins to exceed the Schönberg-Chandrasekhar limit, the shell narrows rapidly. The core contracts and heats up preferentially toward the center to accommodate the release of gravitational energy from central regions; matter outside the narrowing shell expands rapidly outward and cools.

Conditions within the star at a typical point during the shell-narrowing phase are shown in Figure 10 (time $t = 10.3 \times 10^9$ yr). The shell may be thought of as being centered at mass fraction 0.1327 with a thickness of $\Delta M_{\text{sh}}/M_{\text{star}} = 0.018$. That is, 10 per cent of the total energy produced in the star occurs interior to mass fraction 0.126 and 10 per cent occurs beyond mass fraction 0.144. At the shell center, temperature is $T_{\text{sh}} = 20.4 \times 10^6$ ° K, density is $\rho_{\text{sh}} = 285$ gm/cm³, and hydrogen abundance by mass is $X_{\text{H}} = 0.138$.

The distributions of $O^{16}$ and $N^{14}$ between the stellar center and the shell illustrate very clearly that temperatures in the shell have been rising throughout the period of thick-shell burning. That is, a larger and larger fraction of the original $O^{16}$ is converted into $N^{14}$ within the shell as evolution progresses. At the base of the shell 77 per cent of the original $O^{16}$ has been converted into $N^{14}$. The maximum abundance of $He^3$ is now $(X_3)_{max} = 5.35 \times 10^{-3}$, again occurring at mass fraction 0.597, and the $C^{12}$ transition layer has not moved perceptibly.

Absorption in the envelope is relatively small compared to that occurring in more massive stars during the same phase. About 1.25 per cent of the nuclear energy produced in the shell is required to expand envelope layers.

Convection extends over the outer 6.31 per cent of the star's mass. Since the $Li^7$ transition layer occurred at a mass fraction of $\sim$0.975 at the beginning of the shell-narrowing phase, the surface $Li^7$ abundance has now been reduced by a factor of $6.31/2.5 \sim 2.5$ from its "initial" value when the star was on the main sequence. The temperature and density at the base of the convective region are only $T_{BE} = 1.406 \times 10^6$ ° K and $\rho_{BE} = 0.06$ gm/cm$^3$, respectively; hence the total amount of $Li^7$ in the envelope of the star is not being reduced by nuclear burning.

Degeneracy in the core is becoming significant. At the center, where density is $\rho_c = 1.52 \times 10^4$ gm/cm$^3$ and temperature is $T_c = 23.868 \times 10^6$ ° K, the exclusion principle is responsible for 46 per cent of the total pressure.

As evolution progresses, the convective envelope extends rapidly inward and the star shortly begins to rise along the giant branch. The contribution of degeneracy to pressure in the contracting core continues to rise; at the same time, electron conduction facilitates the flow of energy out of the core. As a result, core temperatures begin to drop at $t \sim 10.43 \times 10^9$ yr and continue to drop until the core becomes nearly isothermal. The surface demand for increasing luminosity requires an increase with time of shell temperatures. Hence, the temperatures in the core begin to rise again after near isothermality has been attained.

Conditions within the last computed model, $t = 10.88 \times 10^9$ yr, are shown in Figure 11. The very shallow temperature gradient in the core is manifest. Throughout most of the hydrogen-exhausted core, the shallowness of the temperature gradient is correlated directly with the extent of degeneracy, as measured by the curve $(P_g/P)$. As before, $P$ is the total pressure and $P_g$ is the pressure which would obtain if the perfect-gas equation of state were employed. At the center, $T_c = 27.35 \times 10^6$ ° K, $\rho_c = 9.17 \times 10^4$ gm/cm$^3$, and $P_g/P = 0.236$.

The center of the shell occurs at mass $M_{sh} = 0.1991\ M_\odot$ and has a thickness of approximately $\Delta M_{sh}/M_\odot = 0.0018$. Since temperature and density at the shell center are $T_{sh} = 24.64 \times 10^6$ ° K and $\rho_{sh} = 208$ gm/cm$^3$, the CN cycle reactions now dominate over the $p$-$p$ reactions. Note that 93 per cent of the original $O^{16}$ has been converted into $N^{14}$ at the base of the shell.

As is illustrated by the distribution of composition variables, convection now extends down to mass fraction 0.292, where temperature and density are $T_{BE} = 2.41 \times 10^6$ ° K and $\rho_{BE} = 0.059$ gm/cm$^3$. As a result of convective mixing, surface abundances by mass of $H^1$, $He^3$, $He^4$, $C^{12}$, and $N^{14}$ have become $X_H = 0.693$, $X_3 = 1.62 \times 10^{-3}$, $X_4 = 0.284$, $X_{12} = 3.25 \times 10^{-3}$, and $X_{14} = 1.62 \times 10^{-3}$. The surface $Li^7$ abundance has been reduced from its main-sequence value by a factor of 28.

## IV. STRUCTURAL DETAILS DURING 1.25 $M_\odot$ EVOLUTION

The distribution of variables in the 1.25 $M_\odot$ star at time $t = 5.96 \times 10^7$ yr, shortly after the main-sequence phase begins, is shown in Figure 12. No remarkable differences exist between this distribution of variables and the distribution in the 1 $M_\odot$ star during the same phase of development (see, for comparison, Fig. 5 in Paper I). In fact, in both cases, convection occurs in a small region near the center (occupying a mass fraction of

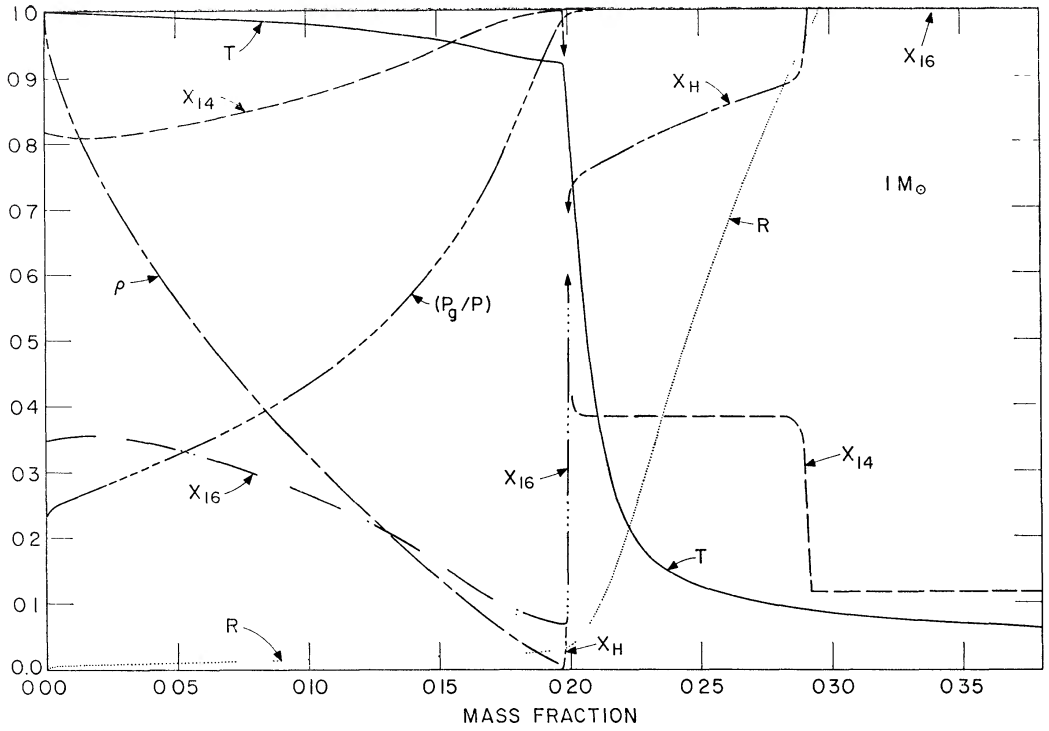


FIG 11 —The variation with mass fraction, for a 1 $M\odot$ star, of state and composition variables when $t = 10\ 8747 \times 10^9$ yr Variables have the same significance and units as in Figs 8–10. Scale limits correspond to $0.0 < \rho < 91171$, $0\ 0 \leq T \leq 27\ 351$, $0\ 0 \leq L \leq 11.422$, $0.0 \leq R \leq 1$, $0\ 0 \leq X_H \leq 0\ 693$, $0\ 0 \leq X_{14} \leq 1.41 \times 10^{-2}$, and $0\ 0 \leq X_{16} \leq 1\ 08 \times 10^{-2}$. Stellar radius is $R_s = 6\ 1784\ R\odot$, and central pressure (not shown) is $6552\ 2 \times 10^{17}$ dyne/cm$^2$ Finally, the ratio of pressure computed in the perfect-gas approximation to the actual pressure with degeneracy included is given by $P_g/P$ and scale limits correspond to $0\ 0 \leq P_g/P \leq 1\ 0$.

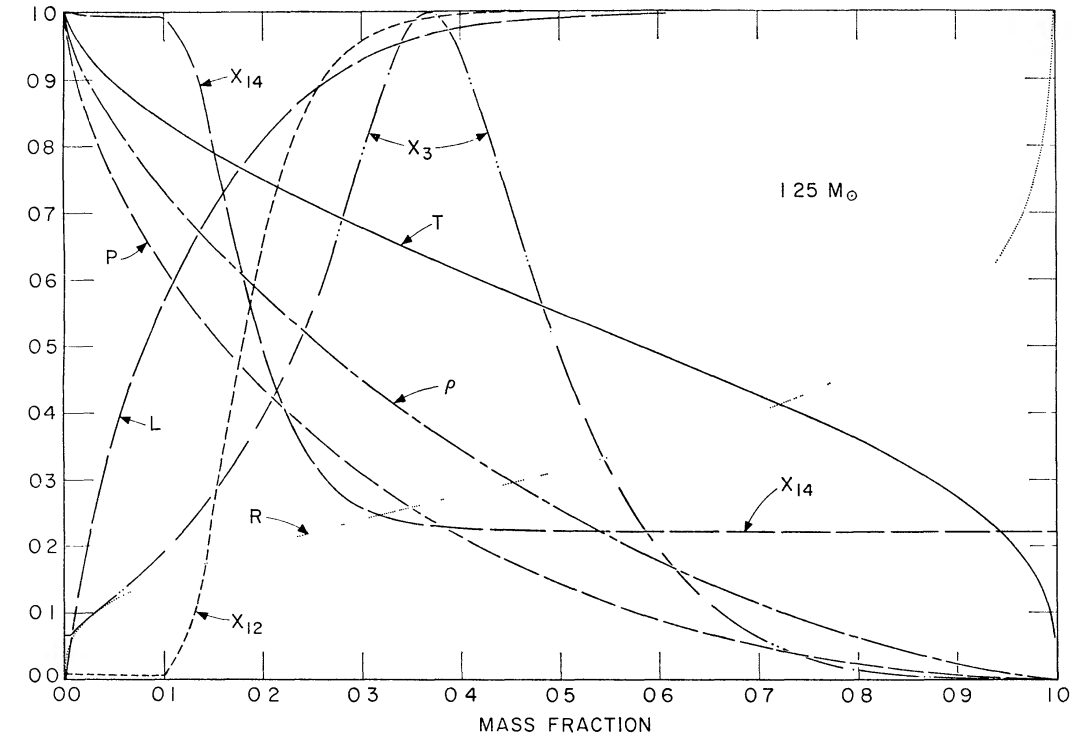


FIG 12 —State and composition variables as a function of mass fraction in a 1.25 $M\odot$ star when $t = 5\ 95972 \times 10^7$ yr Variables have the same significance and units as in Figs 8 and 9. Scale limits correspond to $0\ 0 \leq P \leq 2\ 1075$, $0\ 0 \leq \rho \leq 93\ 621$, $0.0 \leq T \leq 16\ 589$, $0\ 0 \leq L \leq 2\ 3080$, $0.0 \leq R \leq 0\ 8661$, $0.0 \leq X_3 < 3\ 70 \times 10^{-4}$, $0\ 0 \leq X_{12} \leq 3\ 61 \times 10^{-3}$, and $0\ 0 \leq X_{14} \leq 5.43 \times 10^{-3}$. The mass fraction in the static envelope is $7.9899 \times 10^{-4}$, as it is in Figs. 13–17, and stellar radius is $R_s = 1.0806\ R\odot$.

0.00924 in the 1.25 $M_\odot$ star), and both $He^3$ and $C^{12}$ have reached equilibrium values over a large fraction of the energy-producing region. The region of nuclear-energy production is highly extended, thanks again to the predominance of the *p-p* chain reactions.

As the 1.25 $M_\odot$ star evolves, the CN cycle reactions increase in relative importance and, contrary to the 1 $M_\odot$ case, the convective core grows, covering a maximum mass fraction of 0.0460 at time $t = 2.53 \times 10^9$ yr. At time $t = 2.23 \times 10^9$ yr, shortly before the convective core has reached its maximum size, the distribution of variables within the star is as shown in Figure 13.

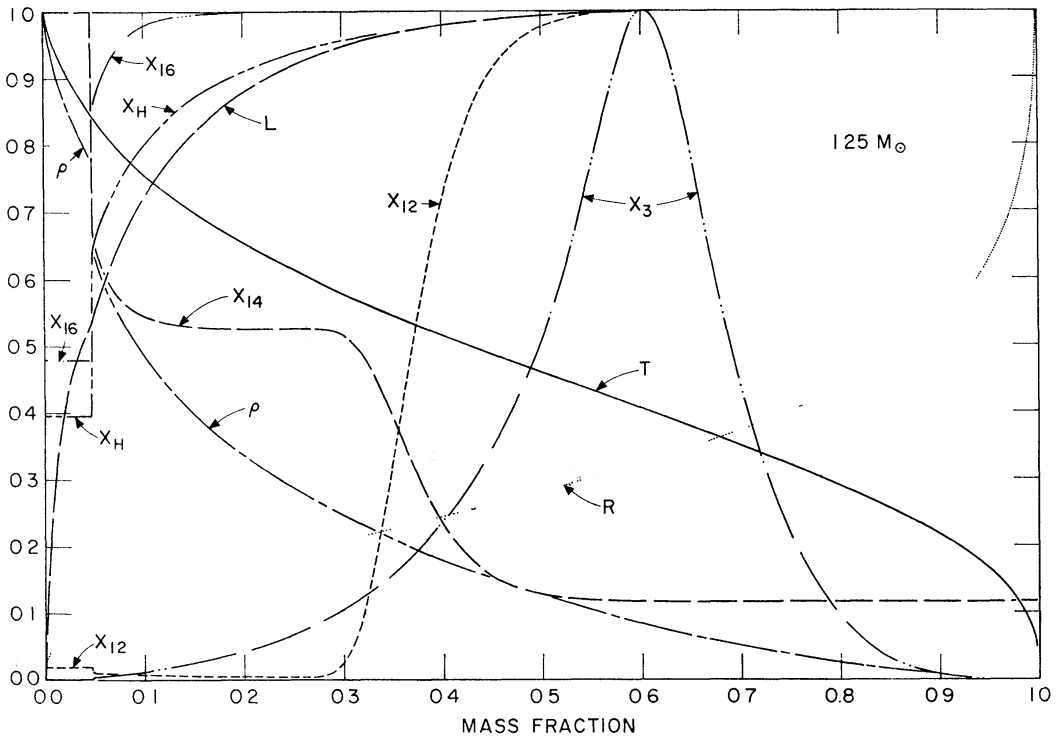


FIG 13.—State and composition variables as a function of mass fraction in a 1.25 $M_\odot$ star when $t = 2.23074 \times 10^9$ yr. Variables have the same significance and units as in previous figures. Scale limits correspond to $0.0 \leq \rho \leq 148.13$, $0.0 \leq T \leq 19.684$, $0\,0 \leq L \leq 3.1390$, $0.0 \leq R \leq 1.0030$, $0.0 \leq X_H \leq 0.708$, $0.0 \leq X_3 \leq 2\,43 \times 10^{-3}$, $0\,0 \leq X_{12} \leq 3.61 \times 10^{-3}$, $0\,0 \leq X_{14} \leq 1.03 \times 10^{-2}$, and $0.0 \leq X_{16} \leq 1\,08 \times 10^{-2}$. The stellar radius is $R_s = 1.2708\ R_\odot$, and central pressure (not shown) is $2.6700 \times 10^{17}$ dyne/cm$^2$.

The most interesting variations occur near the boundary of the convective core. At the boundary itself, density and *all* composition variables change *discontinuously*—primarily as a result of the fact that the mass of the convective core has been steadily increasing. The abundance of $C^{12}$ changes discontinuously for two reasons. Within the core, because of the increased conversion of $O^{16}$ into $N^{14}$, $C^{12}$ is in equilibrium with a higher abundance of $N^{14}$ than is the case just outside the core. In addition, however, $C^{12}$ is in *average* equilibrium in the core whereas it is in local equilibrium outside the core. For a given concentration of $N^{14}$, the equilibrium abundance of $C^{12}$ increases with increasing temperature. Since the average temperature sampled by a typical $C^{12}$ nucleus near the inner edge of the core boundary is higher than the temperatures near the boundary, $C^{12}$ is more abundant at the inner edge than if it were in local equilibrium there. Hence, even if the abundance of $N^{14}$ were constant throughout the interior, the $C^{12}$ abundance would decrease abruptly across the core boundary.

This latter effect is even more pronounced in the case of $He^3$, the only modification being that the equilibrium abundance of $He^3$ decreases with increasing temperature. In the core, $He^3$ is in average equilibrium at an abundance by mass of $\bar{X}_3 = 1.16 \times 10^{-6}$, whereas, just outside the core it is in local equilibrium at an abundance of $X_3 = 4.08 \times 10^{-6}$. It is this jump by a factor of 3.5 in the $He^3$ abundance which accounts for the increase in slope of the luminosity variable across the core boundary.

As final observations, note that the $C^{12}$ transition layer occurs at a mass fraction of about 0.372 and that $He^3$ has reached an abundance of $X_3 = 2.43 \times 10^{-3}$ at a mass fraction of approximately 0.605. The fact that this latter abundance is approximately only one half of the $He^3$ abundance in the 1 $M_\odot$ star at a comparable phase is due primarily to the fact that the average temperatures in the 1.25 $M_\odot$ star are higher than in the 1 $M_\odot$ star.

The mass fraction in the convective core finally begins to decrease when the abundance of hydrogen in the core is reduced to $X_H = 0.184$. As hydrogen near the center is reduced even further, a period of over-all contraction ensues, just as in more massive stars which possess a much larger convective core during the major portion of the core hydrogen-burning phase.

The period of over-all contraction is one of pronounced changes in observable characteristics (see points 3 to 4 for the 1.25 $M_\odot$ track in Fig. 1). It is illuminating to realize that these changes occur for a star which has a negligible convective core when it reaches the main sequence and which produces, when the core attains its maximum size, only half its total energy output in this core.

Toward the end of the over-all contraction phase, central temperatures begin to drop and central densities begin to rise at an extremely rapid rate (see curves $T_c$ and $\rho_c$ versus $t$ in Fig. 5). The distribution of variables in the star during the ensuing shell-development stages, $t = 3.00 \times 10^9$ yr, is shown in Figure 14.

At the center, the abundance of hydrogen is $X_H = 2.78 \times 10^{-3}$ and $\epsilon_{nuc}/\epsilon_{grav} = 29.87$. Here also 82 per cent of the original $O^{16}$ has been converted into $N^{14}$. The $C^{12}$ transition layer is at mass fraction 0.376 and the position of maximum $He^3$ abundance is still at mass fraction 0.605, where $X_3 = 2.82 \times 10^{-3}$.

The evolution of the 1.25 $M_\odot$ star following the formation of a shell source is quite similar to the evolution of the 1 $M_\odot$ star. The only significant differences are in the magnitude of the luminosity drop during the shell-narrowing phase and in the magnitude of the central temperature drop which occurs when degeneracy becomes important in the hydrogen-exhausted core. The fact that changes are more pronounced in the 1.25 $M_\odot$ star is due to the fact that, after the effective Schönberg-Chandrasekhar limit is reached, the 1 $M_\odot$ star is much closer to the base of the giant branch than is the 1.25 $M_\odot$ star.

The similarity between 1 $M_\odot$ and 1.25 $M_\odot$ structure following the development of a shell source is demonstrated by Figures 15–17, which are to be compared with Figures 9–11.

Figure 15 illustrates the distribution of variables in the 1.25 $M_\odot$ star at $t = 3.55 \times 10^9$ yr, approximately midway through the phase of hydrogen burning in a thick shell. As in the 1 $M_\odot$ case, the hydrogen-exhausted core is quite isothermal. The shell is "centered" at a mass fraction 0.082 and has a thickness $\Delta M_{sh}/M_{star} \cong 0.133$, compared to a thickness of 0.172 in the 1 $M_\odot$ star at approximately the same stage. Temperature and density at the shell center are approximately $T_{sh} = 18.80 \times 10^6$ ° K and $\rho_{sh} = 137$ gm/cm$^3$, so that hydrogen burning still proceeds primarily through the $p$-$p$ chains.

Conditions in central regions of the 1.25 $M_\odot$ star at $t = 4.19 \times 10^9$ yr are shown in Figure 16. The star has just reached the base of the giant branch, and the central temperature has just begun to drop. Convection carries energy over the outer 8.96 per cent of the star's mass. Note that, during the preceding shell-narrowing phase, a sizable temperature gradient has built up between the stellar center and the shell. The shell is centered at mass fraction 0.127 and has a thickness $\Delta M_{sh}/M_{star} = 0.00640$. Temperature

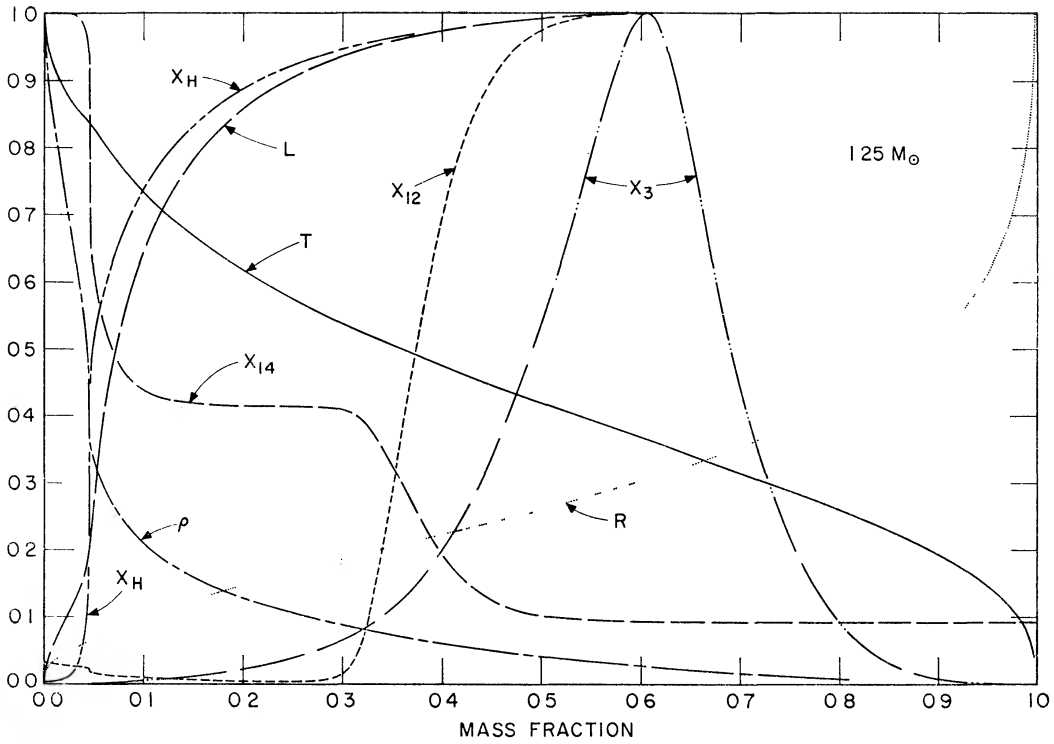


FIG. 14 —State and composition variables as a function of mass fraction in a 1.25 $M\odot$ star when $t = 3.00224 \times 10^9$ yr. Variables have the same significance and units as in previous figures. Scale limits correspond to $0\,0 \leq P \leq 6\,1921$, $0.0 \leq \rho \leq 431.97$, $0.0 \leq T \leq 22.473$, $0\,0 \leq L \leq 4.0746$, $0.0 \leq R \leq 1\,0689$, $0\,0 \leq X_H \leq 0\,708$, $0\,0 \leq X_3 \leq 2.82 \times 10^{-3}$, $0\,0 \leq X_{12} \leq 3.61 \times 10^{-3}$, and $0\,0 \leq X_{14} \leq 1.31 \times 10^{-2}$ Stellar radius is $R_s = 1.3830\ R\odot$.

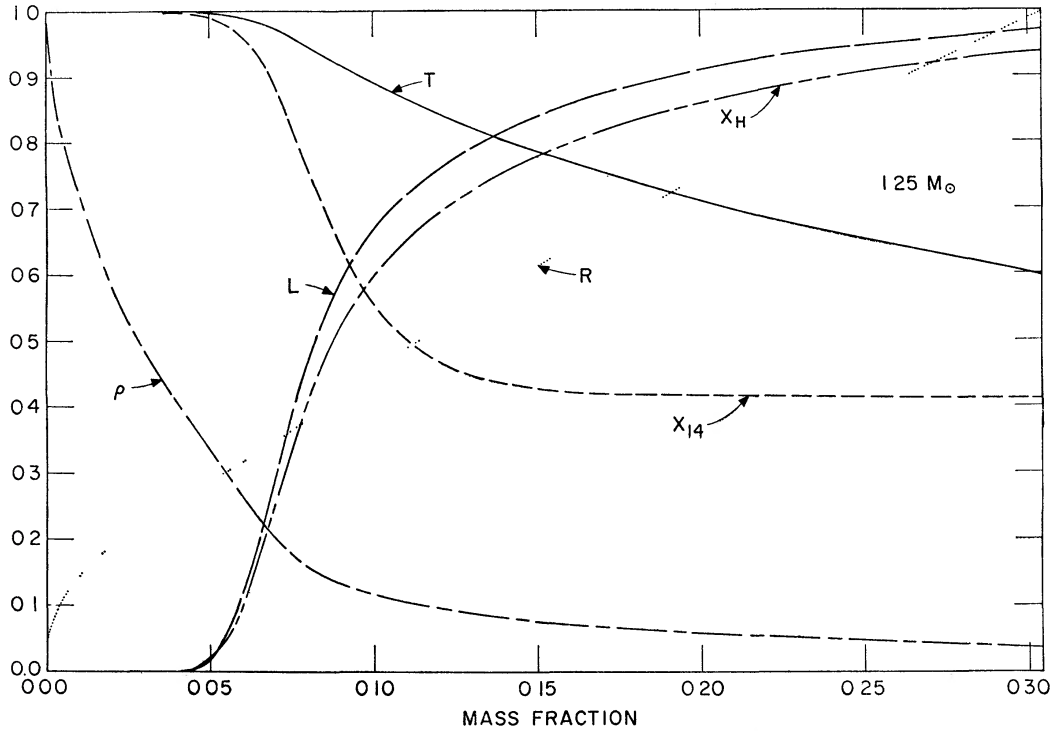


FIG. 15 —State and composition variables as a function of mass fraction in a 1.25 $M\odot$ star when $t = 3.55240 \times 10^9$ yr. Variables have the same significance and units as in Fig. 11. Scale limits correspond to $0.0 \leq \rho \leq 896.04$, $0.0 \leq T \leq 19\,991$, $0.0 \leq L \leq 4.9165$, $0\,0 \leq R \leq 0.2$, $0.0 \leq X_H \leq 0\,708$, and $0.0 \leq X_{14} \leq 1.31 \times 10^{-2}$. Stellar radius is $R_s = 1.5835\ R\odot$, and central pressure (not shown) is $11.840 \times 10^{17}$ dyne/cm$^2$.

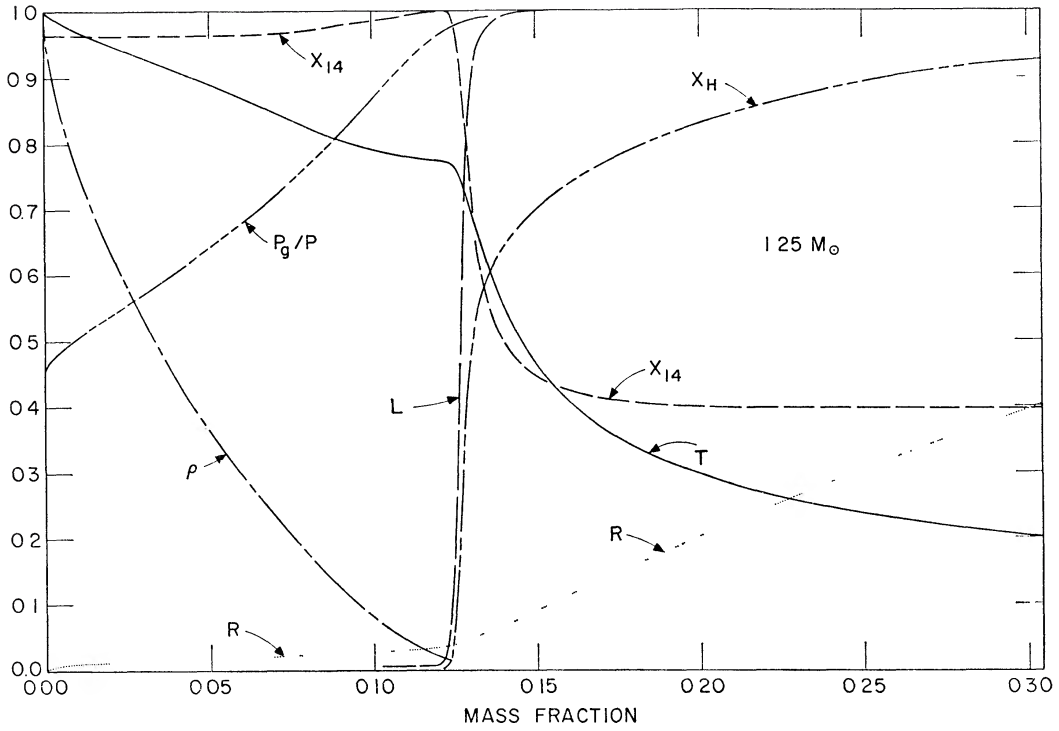


FIG 16.—State and composition variables as a function of mass fraction in a 1 25 $M_{\odot}$ star when $t = 4.18872 \times 10^{9}$ yr. Variables have the same significance and units as in Fig 11 Scale limits correspond to $0\,0 \leq \rho \leq 30478$, $0.0 \leq T \leq 29\,207$, $0\,0 \leq L \leq 5.2339$, $0.0 \leq R \leq 1\,0$, $0\,0 \leq X_{H} \leq 0.708$, $0\,0 \leq X_{14} \leq 1\,36 \times 10^{-2}$, and $0.0 \leq P_g/P \leq 1\,0$. Stellar radius is $R_s = 3.1148\ R_{\odot}$, and central pressure (not shown) is $1214\,1 \times 10^{17}$ dyne/cm$^2$.

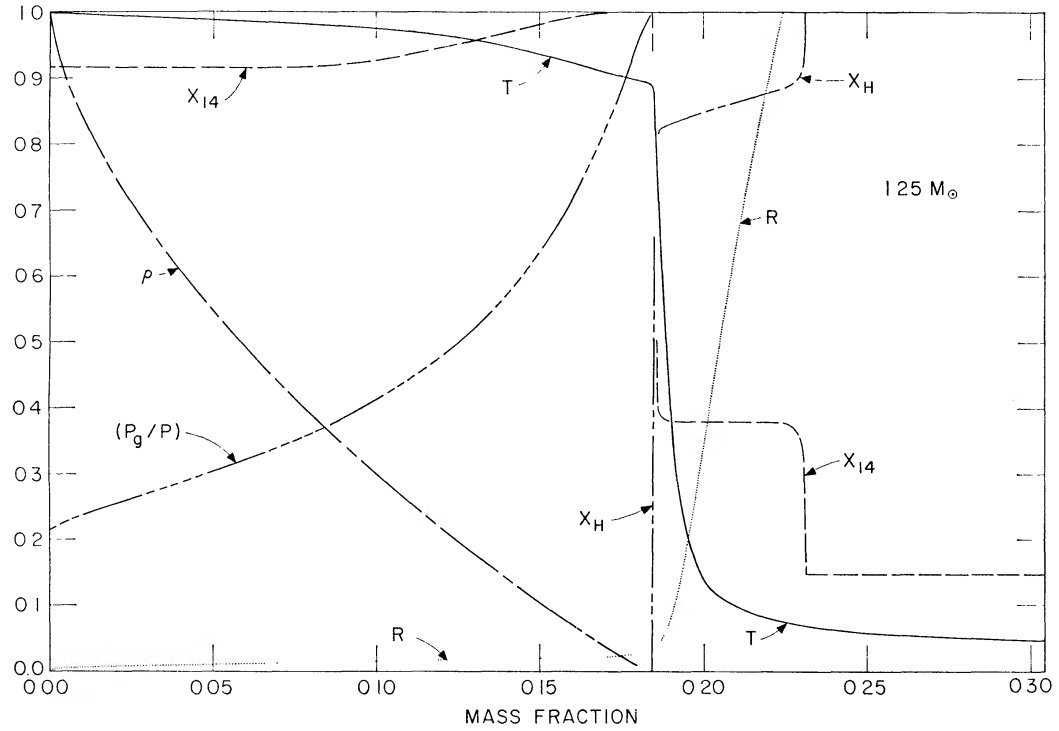


FIG 17.—State and composition variables as a function of mass fraction in a 1.25 $M_{\odot}$ star when $t = 4.53752 \times 10^{9}$ yr. Variables have the same significance and units as in Fig. 16 Scale limits correspond to $0\,0 \leq \rho \leq 129492$, $0.0 \leq T \leq 31\,041$, $0\,0 \leq R \leq 1.0$, $0\,0 \leq X_{H} \leq 0\,693$, $0\,0 \leq X_{14} \leq 1.43 \times 10^{-2}$, and $0\,0 \leq P_g/P \leq 1.0$. Stellar radius is $R_s = 10\,322\ R_{\odot}$, central pressure (not shown) is $11636 \times 10^{17}$ dyne/cm$^2$, and surface luminosity is 29 010 $L_{\odot}$.

and density at the shell center are $T_{sh} = 21.91 \times 10^6$ ° K and $\rho_{sh} = 241$ gm/cm³. The CN cycle reactions have therefore begun to surpass the $p$-$p$ reactions in effectiveness. At the center, where $P_g/P = 0.46$, the electron pressure is ~2.8 times larger than would be the case if degeneracy had been neglected.

Conditions in the last model computed, $t = 4.54 \times 10^9$ yr, are shown in Figure 17. The star is now well advanced along the giant branch and the hydrogen-exhausted core has again become relatively isothermal. Electron degeneracy at the center increases the electron pressure there by a factor of ~6.6 over that computed via the perfect-gas law. The shell is centered at mass fraction 0.185 and shell thickness is $\Delta M_{sh}/M_{star} = 8.96 \times 10^{-4}$. At the shell center, $T_{sh} = 27.20 \times 10^6$ ° K and $\rho_{sh} = 142$ gm/cm³, and energy production is primarily via the CN cycle reactions.

Note that the convective envelope now extends down to a mass fraction of 0.232. As a result of convective mixing during the passage up the giant branch, the surface abundances have become in this last model: $X_H = 0.693$, $X_3 = 9.07 \times 10^{-4}$, $X_4 = 0.284$, $X_{12} = 2.84 \times 10^{-3}$, and $X_{14} = 2.09 \times 10^{-3}$. The surface abundance of $O^{16}$ has not changed. By the end of the period of thick-shell burning, $Li^7$ is destroyed over all but the outer 1.73 per cent of the star's mass. The surface $Li^7$ abundance begins to drop before the star reaches the base of the giant branch. In the last model, the surface $Li^7$ abundance has been depleted by a factor of about 43 relative to its main-sequence value.

## V. STRUCTURAL DETAILS DURING 1.5 $M_\odot$ EVOLUTION

Structural characteristics in the 1.5 $M_\odot$ star are qualitatively identical with those in the 1.25 $M_\odot$ star at comparable phases. Conditions within the 1.5 $M_\odot$ star on reaching the main sequence are described in Paper I.

The distribution of variables in Figure 18 illustrates conditions in the 1.5 $M_\odot$ star at $t = 9.40 \times 10^8$ yr, shortly after the mass fraction in the convective core has reached its maximum during the core hydrogen-burning phase. Near the boundary of the convective core, the near-discontinuity in density, in the luminosity slope, and in all composition variables is again occasioned in part by the fact that core mass has been increasing. Energy production is more concentrated toward the center than in the 1.25 $M_\odot$ case, a reflection of the greater importance of the CN cycle reactions in the 1.5 $M_\odot$ star.

In Figure 19, conditions within the star are shown during the shell-narrowing phase at $t = 2.07 \times 10^9$ yr, just before central temperatures begin to drop as a result of increasing electron degeneracy. The temperature gradient between center and shell is somewhat steeper and absorption in the expanding envelope is somewhat more pronounced than in the 1.25 $M_\odot$ case. The hydrogen-burning shell is centered at mass fraction 0.116, where $T_{sh} = 22.90 \times 10^6$ ° K and $\rho_{sh} = 196$ gm/cm³, and shell thickness is $\Delta M_{sh}/M_{star} = 0.0103$. In the hydrogen-exhausted core, 89 per cent of the original $O^{16}$ has been converted into $N^{14}$.

During the period preceding the growth of a convective envelope, $Li^7$ is destroyed over all but the outer 1.43 per cent of the star's mass. Since convection now covers the outer 1.78 per cent of the star's mass, the surface $Li^7$ abundance has been reduced by a factor of 1.24 relative to its value when the star reaches the main sequence.

Conditions in the last model constructed, $t = 2.27 \times 10^9$ yr, are shown in Figure 20. Interior variations within the star are so similar to those in the 1.25 $M_\odot$ and 1 $M_\odot$ stars during the giant phase that very little comment is necessary. The shell is centered at mass fraction 0.146, where $T_{sh} = 26.02 \times 10^6$ ° K and $\rho_{sh} = 161$ gm/cm³. Shell thickness is $\Delta M_{sh}/M_{star} = 9.10 \times 10^{-4}$. The convective envelope covers the outer 73.4 per cent of the star's mass and surface abundances of $H^1$, $He^3$, $C^{12}$, and $N^{14}$ have become $X_H = 0.702$, $X_3 = 6.07 \times 10^{-4}$, $X_{12} = 2.89 \times 10^{-3}$, and $X_{14} = 2.04 \times 10^{-3}$. The surface $Li^7$ abundance is down by a factor of 51 relative to its main-sequence value.

A final comparison of relative lifetimes during various phases is made in Table 2 between the 1.25 $M_\odot$ and 1.5 $M_\odot$ stars and the 3.0 $M_\odot$ star described in Paper II.

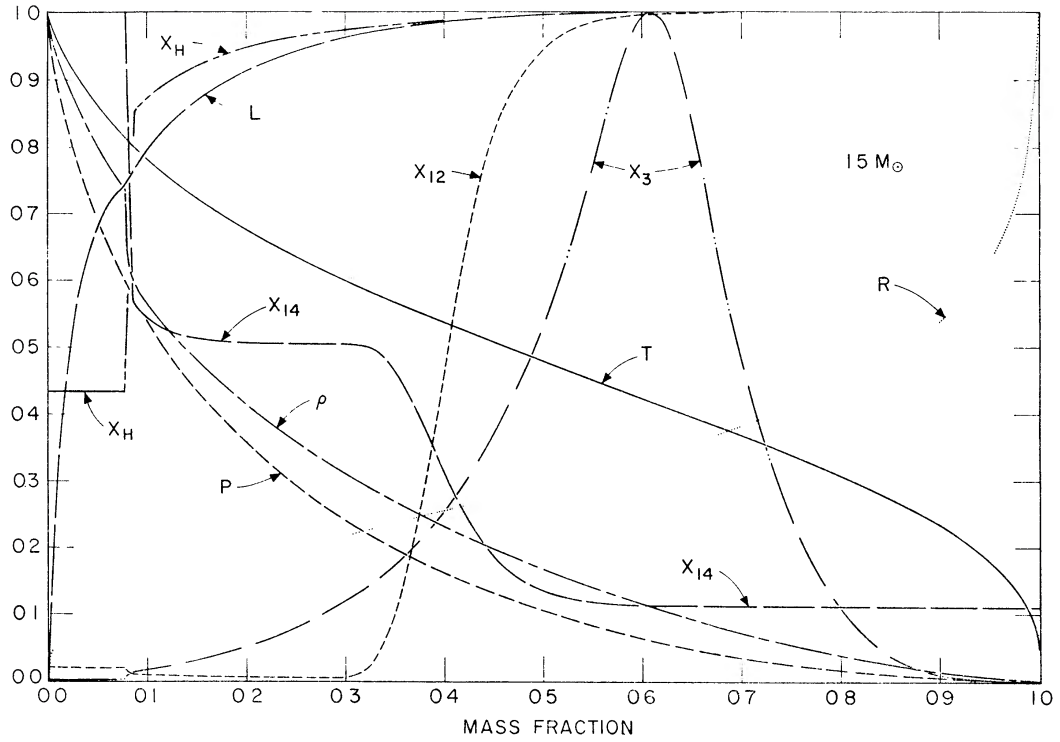


FIG. 18 —State and composition variables as a function of mass fraction in a 1.5 $M\odot$ star when $t = 9\ 39715 \times 10^8$ yr. Variables have the same significance and units as in Figs 8 and 9. Scale limits correspond to $0.0 \leq P \leq 2.1954, 0\ 0 \leq \rho \leq 103.51, 0\ 0 \leq T \leq 20.323, 0\ 0 \leq L \leq 6\ 4563, 0.0 \leq R \leq 1.0758$, $0\ 0 \leq X_H \leq 0.708, 0\ 0 \leq X_3 \leq 1\ 41 \times 10^{-3}, 0\ 0 \leq X_{12} \leq 3.61 \times 10^{-3}, 0.0 \leq X_{14} \leq 0\ 0107$. The mass fraction in the static envelope is $6.78029 \times 10^{-4}$, as it is in Figs. 19 and 20, and stellar radius is $R_s = 1.3713\ R\odot$.

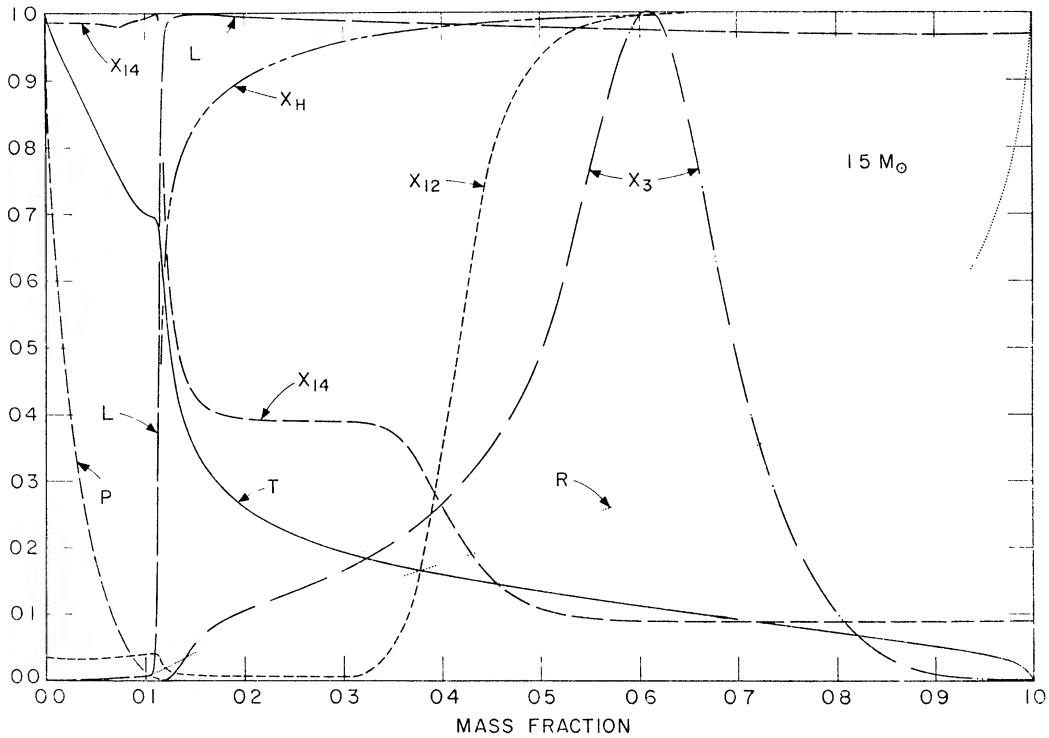


FIG. 19.—State and composition variables as a function of mass fraction in a 1.5 $M\odot$ star when $t = 2\ 07146 \times 10^9$ yr Variables have the same significance as in Figs. 8 and 9. Scale limits correspond to $0.0 \leq P \leq 1288.1$, $0.0 \leq T \leq 34.052$, $0.0 \leq L \leq 9.6348$, $0.0 \leq R \leq 3\ 3426$, $0.0 \leq X_H \leq 0\ 708$, $0\ 0 \leq X_3 \leq 1.95 \leq 10^{-3}$, $0\ 0 \leq X_{12} \leq 3.61 \times 10^{-3}$, and $0\ 0 \leq X_{14} \leq 1\ 39 \times 10^{-2}$. The stellar radius is $R_s = 3\ 6359\ R\odot$, and central density (not shown) is 30738 gm/cm³.

Entries for each star give the percentage of time spent by that star in the indicated phase relative to the total time from formation to the base of the red-giant branch (points 10 in Fig. 1 and point 10 in Fig. 1 of Paper II). The most interesting comparison is the fraction of time spent in the phase of hydrogen burning in a thick shell. This fraction increases rapidly with decreasing mass, a result which is due primarily to the fact that, as mass decreases, hydrogen is exhausted over a smaller fraction of the star's mass when the central hydrogen abundance becomes effectively zero.

Two other factors contribute to the longer relative time spent by smaller masses in

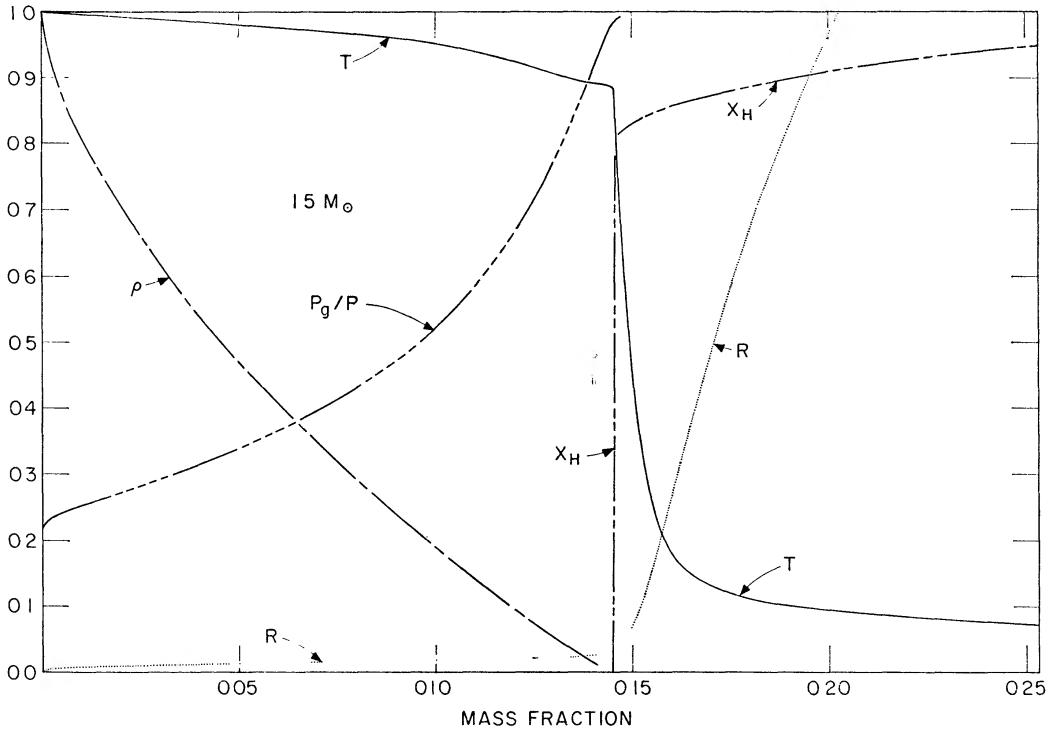


FIG. 20.—State and composition variables as a function of mass fraction in a 1 5 $M_\odot$ star when $t$ = 2.2683 × $10^9$ yr. Variables have the same significance and units as in Fig. 11 Scale limits correspond to 0 0 ≤ $\rho$ ≤ 113668, 0 0 ≤ $T$ ≤29.896, 0 0 ≤ $R$ ≤ 1 0, 0 0 ≤ $X_H$ ≤ 0 702, and 0 0 ≤ $P_g/P$ ≤ 1 0. Stellar radius is $R_s$ = 7 7239 $R_\odot$, central pressure (not shown) is 9 4082 × $10^{20}$ dyne/cm², and surface luminosity is $L_s$ = 19 613 $L_\odot$

TABLE 2

RELATIVE LIFETIMES

| PHASE DESCRIPTION | PERCENTAGE OF LIFETIME TO BASE OF RED-GIANT BRANCH | | |
|---|---|---|---|
| | 1 25 $M_\odot$ | 1 5 $M_\odot$ | 3 0 $M_\odot$ |
| To main sequence | 0 7 | 0 9 | 1 0 |
| Core hydrogen burning | 66 6 | 75 1 | 89 0 |
| Over-all contraction plus shell development | 4 3 | 3 9 | 4 2 |
| Thick hydrogen-burning shell | 24 8 | 16 9 | 4 1 |
| Shell narrowing to base of giant branch | 3 5 | 3 2 | 1 8 |

the thick shell-burning phase. They are: (1) the more gradual variation with mass fraction of the molecular weight through the shell, and (2) the greater relative importance of electron degeneracy in the hydrogen-exhausted core. Both factors have the effect of increasing the Schönberg-Chandrasekhar limit and thus permit the shell to move through a larger mass fraction before the star must adopt a giant structure. The dependence of the effective limit on stellar mass may be estimated. At the start of the shell-narrowing phase (points 7 in Fig. 1 and point 6 in Fig. 1 of Paper II), the shell is centered at a mass fraction of $\sim$0.100, 0.106, 0.112, and 0.125 for stars of mass $M/M_\odot$ = 3.0, 1.5, 1.25, and 1.0, respectively. Toward the end of the shell-narrowing phase (points 10 in Fig. 1) in stars of mass $M/M_\odot$ = 3.0, 1.5, 1.25, and 1.0, the mass fraction in the hydrogen exhausted core is 0.110, 0.121, 0.126, and 0.136, respectively. The effective Schönberg-Chandrasekhar limit may be thought of as lying between these two sets of values.

## VI. OBSERVATIONAL CONSEQUENCES

### *a) Surface Lithium Abundance*

In previous sections it was mentioned that, prior to the giant phase, $Li^7$ (and also $Li^6$) is destroyed over most of the interior of all three stars, leaving only a very thin surface layer over which lithium retains its main-sequence abundance. During the shell-development stage, as each star approaches the base of its red-giant track, the lithium in this thin layer is spread over a growing convective envelope, resulting in a reduction in the surface lithium concentration.

The circled numbers along each track in Figure 1 denote the factors by which the surface $Li^7$ abundance is reduced relative to the surface $Li^7$ abundance which characterizes the star on the main sequence. Note that, between $\log T_e = 3.72$ and $\log T_e = 3.67$, the reduction factor is *roughly* the same function of surface temperature for all three stars. The rapidity with which the surface lithium abundance drops with decreasing surface temperature in this range, coupled with the approximate magnitude independence of the reduction factor, suggests that an observational test is quite feasible. To facilitate interpretation of observational results, the surface temperature dependence of the lithium depletion is given in Figure 21. From this figure, along with Figures 2–7, it is possible to determine, for any surface temperature, the magnitude dependence of the surface depletion. It should be cautioned that quantitative results are definitely model-dependent and that it is therefore of considerable value to obtain, *from the observations*, the surface temperature and magnitude dependence of surface Li depletion.

### *b) The Production of $He^3$ in Ordinary Stars*

In meteorites the relative abundance by mass of $He^3$ to $He^4$ is about $2 \times 10^{-4}$. In the past, the possibility that such a large ratio of $He^3$ to $He^4$ could be achieved in stars was overlooked. This oversight was based on the observation that, in regions of strong hydrogen burning, the equilibrium abundance by mass of $He^3$ is much smaller than $10^{-4}$. For example, at the center of the 1.5 $M_\odot$ model described in Figure 18, $X_3 = 2.3 \times 10^{-6}$. At the shell center in the 1.5 $M_\odot$ model described in Figure 20, $X_3 = 2.3 \times 10^{-8}$. Further, in the normal course of events, $He^3$ vanishes at the same time that hydrogen vanishes.

In this paper, as well as in Papers I–V, it has been shown that, outside of the region of major $He^4$ production, $He^3$ builds up to abundances considerably larger than those found in the regions of significant nuclear-energy generation. An estimate of the total mass of $He^3$ in the last model of each mass described in Papers II–IV as well as in the last model of each mass discussed in this paper is given in Table 3. Results for a 2.25 $M_\odot$ model have also been included. Entries are given in units of $10^{-4}$ $M_\odot$.

It is clear by inspection that, for masses $M \leq 2.25$ $M_\odot$, the ratio of newly formed $He^3$ to newly formed $He^4$ in the star is considerably in excess of $2 \times 10^{-4}$. Such is the case also for the more massive stars.

Certainly, many things will occur to alter the $He^3/He^4$ ratio as the star evolves and the exhibited "overabundance" of newly formed $He^3$ to newly formed $He^4$ may or may not persist throughout the lifetime of each star, or, more importantly, occur in the matter which is returned by the star to the interstellar medium. It does seem likely, however, that a considerable fraction of the $He^3$ in the interstellar medium of our Galaxy may well have been formed in stars.

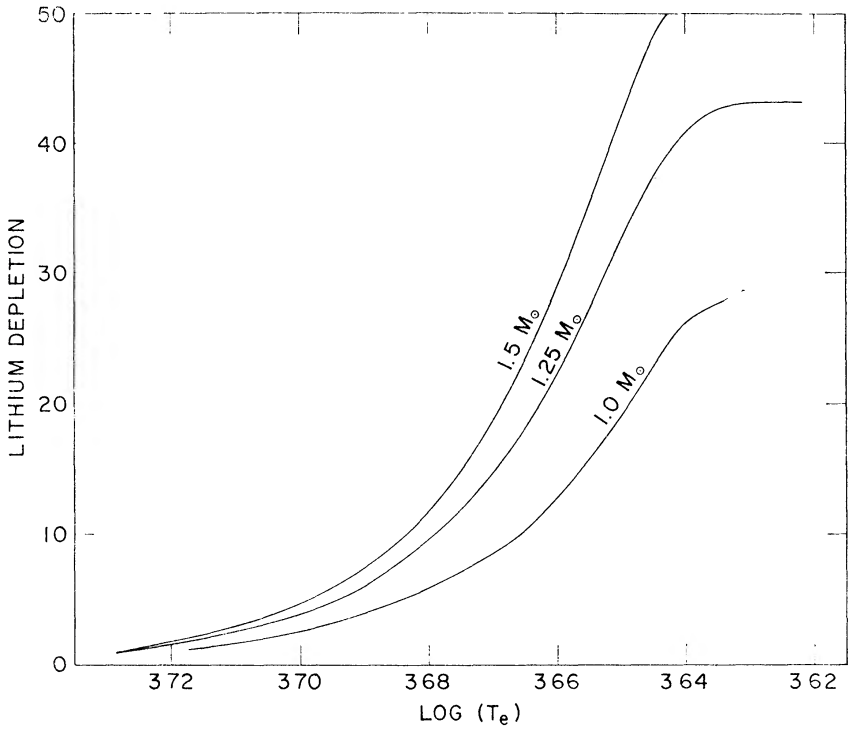


FIG. 21.—Lithium depletion as a function of surface temperature for stars of mass $M/M\odot = 1, 1.25$, and 1.5. The ordinate gives the factor by which the surface $Li^7$ abundance by mass has been reduced from its main-sequence value.

TABLE 3

TOTAL MASS OF $He^3$ IN MODEL STARS ($10^{-4}\ M\odot$)

| $M_{star}/M\odot$ | 1 | 1.25 | 1.5 | 2.25 | 3 | 5 | 9 |
|---|---|---|---|---|---|---|---|
| $M(He^3)/(10^{-4}\ M\odot)$ | 10.5 | 8.7 | 6.7 | 4.6 | 3.2 | 2.0 | 1.2 |

It has been recently suggested (Faulkner 1966; Faulkner and Iben 1966) that the $He^4$ abundance in the oldest stars in the Galaxy may be considerable. The inference is that this $He^4$ must have been formed either during the early stages of galactic history in supermassive stars or during a more condensed phase of the proto-Universe. Detailed calculations (Fowler, Hoyle, and Wagoner 1966) show that the $He^3/He^4$ ratio formed in supermassive stars is negligible compared to the value $2 \times 10^{-4}$ quoted for meteorites.

It is intriguing to speculate that the further development of the practical theory of stellar evolution may divulge that stars produce and return to the interstellar medium a $He^3/He^4$ ratio far in excess of the ratio which presently occurs in galactic gas. One would then be in a position to state by an independent argument that only a small fraction of the original $He^4$ in our Galaxy was formed in ordinary stars.

### *c) Evidence from Old Population I Clusters in Support of the Detailed Theory of Stellar Evolution*

Cluster diagrams formed by stars in NGC 188 and M67, respectively, are reproduced in Figure 22 (observations by Sandage 1962) and in Figure 23 (observations by Johnson and Sandage 1955). The solid curves in each figure are simple "eye-fit" attempts to replace the observed distributions by reasonable mean representations. Although it is hoped that these curves are predominantly unbiased, it must be admitted that the "gap" occurring in the adopted mean for M67 has been strongly influenced by the fact that stars which possess a convective core during core hydrogen burning exhibit an extremely pronounced and *rapid* change in luminosity during the phase of over-all contraction.

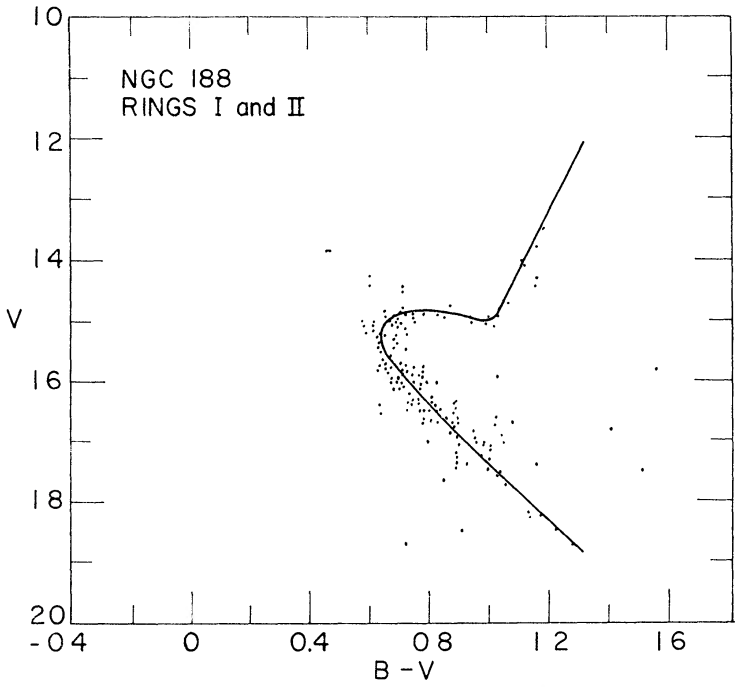


FIG. 22.—The Hertzsprung-Russell diagram of the cluster NGC 188 as reproduced from Sandage (1962). The solid curve is an eye-fitted mean.

The rapidity of changes during the phase of over-all contraction, *relative* to rates of change during both the preceding and the following phase, suggests an effective discontinuity in the stellar density distribution for metal-rich clusters which are young enough to contain stars with convective cores.

Despite the admitted bias, it seems incontrovertible that the density of stars between the end points of the chosen gap in Figure 23 is much less than elsewhere along the mean curves. To be more emphatic, the existence of a gap shall here be accepted as an observational fact which serves as a very strong corroboration of the detailed theory of stellar evolution during pure hydrogen-burning stages.

The curves in Figure 24 represent a venture in transforming, into a theoretical H-R diagram, portions of the mean curves drawn in Figures 22 and 23. Bolometric corrections and the $B - V$ to $\log T_e$ transformation have been taken from Arp (1958) as represented by the mean curves in Figure 1-1 of Hayashi, Hōshi, and Sugimoto (1962). The absolute magnitudes of stars in each cluster have been assigned in such a way as to bring the main-sequence portions of the clusters into coincidence. This procedure of forcing coinci-

dence is not necessarily valid but is admissible in the absence of any precise knowledge of surface abundances and of interstellar reddening and absorption.

In the observer's diagram, the subgiant branches in both M67 and NGC 188 slope downward toward redder colors; in the transformed diagram, the subgiant branch in NGC 188 is essentially horizontal and in fact slopes slightly upward toward the red. The magnitude and sense of the distinct difference between M67 and NGC 188 in the slope of the subgiant branch is an additional confirmation of the qualitative correctness of the detailed theory of stellar evolution. From Figure 1 and from the discussion in § II, it is clear that the luminosity drop during the shell-narrowing phase (points 7 to 10) decreases with decreasing mass, becoming nearly horizontal in the neighborhood of

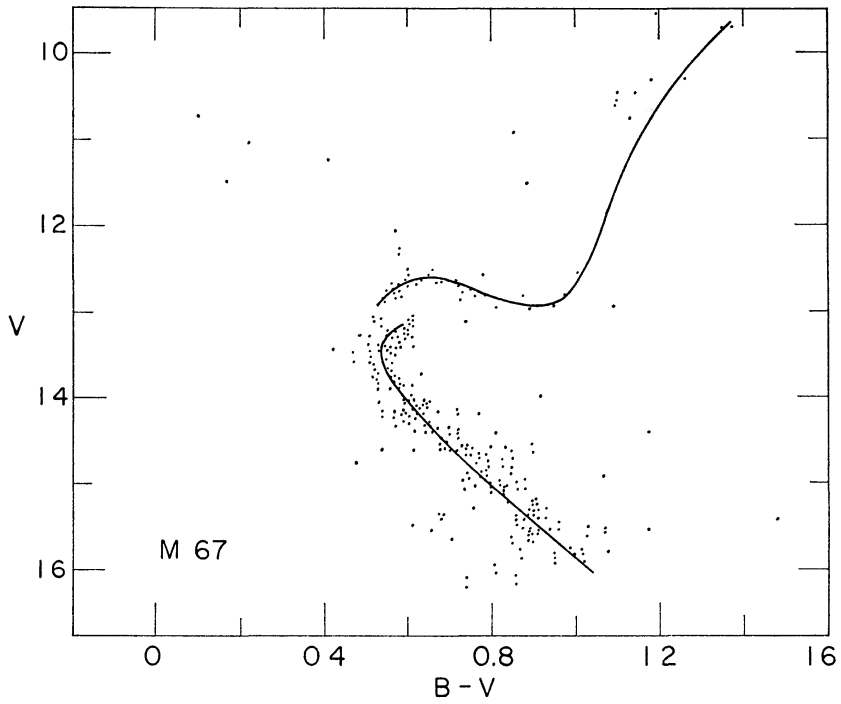


FIG. 23.—The Hertzsprung-Russell diagram of the cluster M67 as reproduced from Johnson and Sandage (1955). The solid curve is an eye-fitted mean.

1 $M_{\odot}$. The mass dependence of the luminosity drop will be reflected in theoretical time-constant loci in such a way that the slope of the theoretical subgiant branch will decrease with increasing assigned age. For the composition employed in this paper, the sign of the theoretical subgiant slope ($= d \log L/d \log T_e$) will change from positive to negative for assigned ages in the neighborhood of $10^{10}$ yr.

As still further observational support for the detailed theory of stellar evolution, note that, at any given luminosity, the giant branch in the younger cluster (M67) is considerably bluer than the giant branch in the older cluster (NGC 188). Again, from the individual paths in Figure 1, it is evident that theoretical time-constant loci will possess this same property. It is highly interesting that this property of cluster age is not due to composition differences. The fact that, at any given luminosity, the older globular-cluster giant branches are much bluer than the giant branches of population I clusters is an independent confirmation of the low metal content of globular cluster stars.

In closing, an estimate of the ages of M67 and NGC 188 will be attempted. The result for NGC 188 will not be significantly different from the age of $12 \times 10^9$ years estimated

recently by Demarque and Larson (1964). However, the method of determination will be sufficiently different that the result may be considered an independent check.

The major drawback in an attempted quantitative comparison of the present theoretical results with the observed cluster diagrams is the faulty theoretical surface temperatures occasioned by a use of opacities from which line absorption has been omitted. The error is in the sense of too high surface temperatures and amounts to roughly $\Delta(\log T_e) = 0.03$–$0.01$ in the range of interest here (see, e.g., Iben 1963). Additional unknown sources of error lie in the choice of parameters in the treatment of envelope convective flow and in the transformation from $B - V$ to $\log T_e$. On the observational side, the extent of reddening is an unknown quantity.

In an effort to bypass these difficulties, use will be made of the gap in M67 and of the slope of the subgiant branch in NGC 188. The existence of a pronounced gap in M67 requires that the cluster be so placed that the luminosity level of the gap is at least as high as the luminosity at which convective cores are important in theoretical models. The luminosity level of the subgiant branch in NGC 188 must be placed in the neighborhood

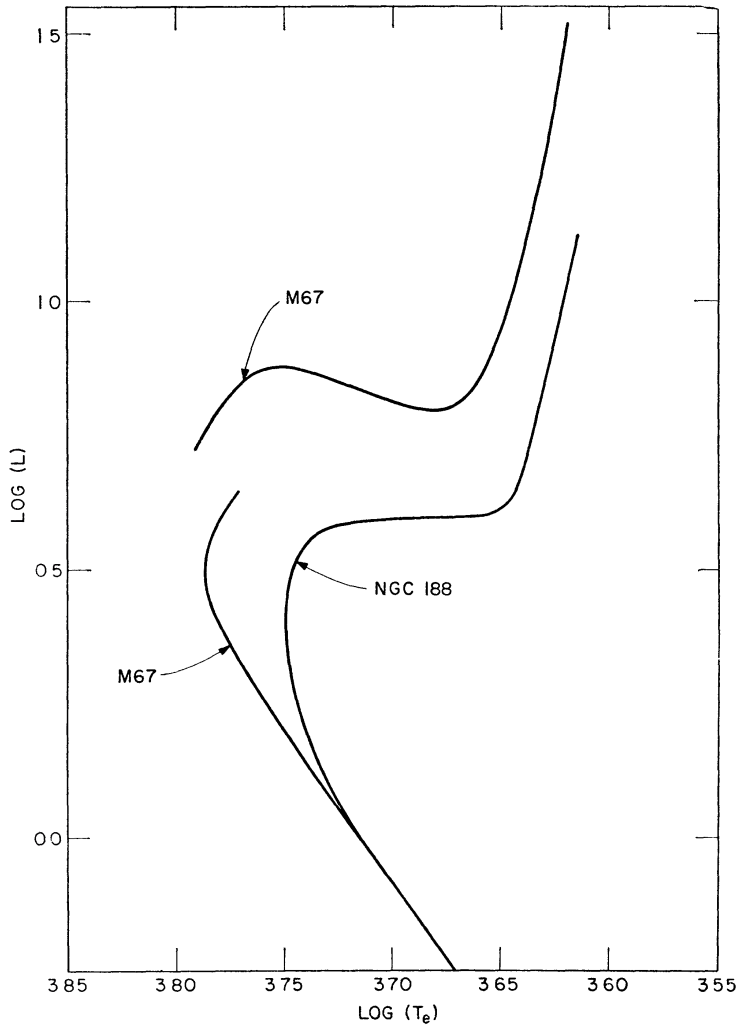


FIG. 24 —The transformed Hertzsprung-Russell diagram for M67 and NGC 188. Main-sequence portions of the clusters have been forced to coincide, and the zero point in the luminosity scale is arbitrary.

of that luminosity for which individual theoretical tracks no longer exhibit a strong luminosity drop during the shell-narrowing phase. Finally, to compensate for the error in theoretical surface temperatures, the cluster diagrams may be moved over bodily to higher surface temperatures. This latter device is not to be interpreted as distrust in and arbitrary manipulation of the observations; it is simply a less time-consuming equivalent of redoing the theoretical model calculations with better opacities.

Results of the stated operations are shown in Figure 25, along with the 1.25 $M_\odot$ and 1.0 $M_\odot$ tracks from Figure 1. The heavy dashed curves and the heavy dot-dash curves correspond to stars in M67 and NGC188, respectively, when the surface temperature at each point along the curves in Figure 24 is moved over uniformly by $\Delta(\log T_e) = 0.0275$. The corresponding thin curves result when surface temperatures are increased uniformly by $\Delta(\log T_e) = 0.0175$. The numbers beside the points along the 1 $M_\odot$ path denote the time in $10^9$ yr required by the star to reach each point from time of formation.

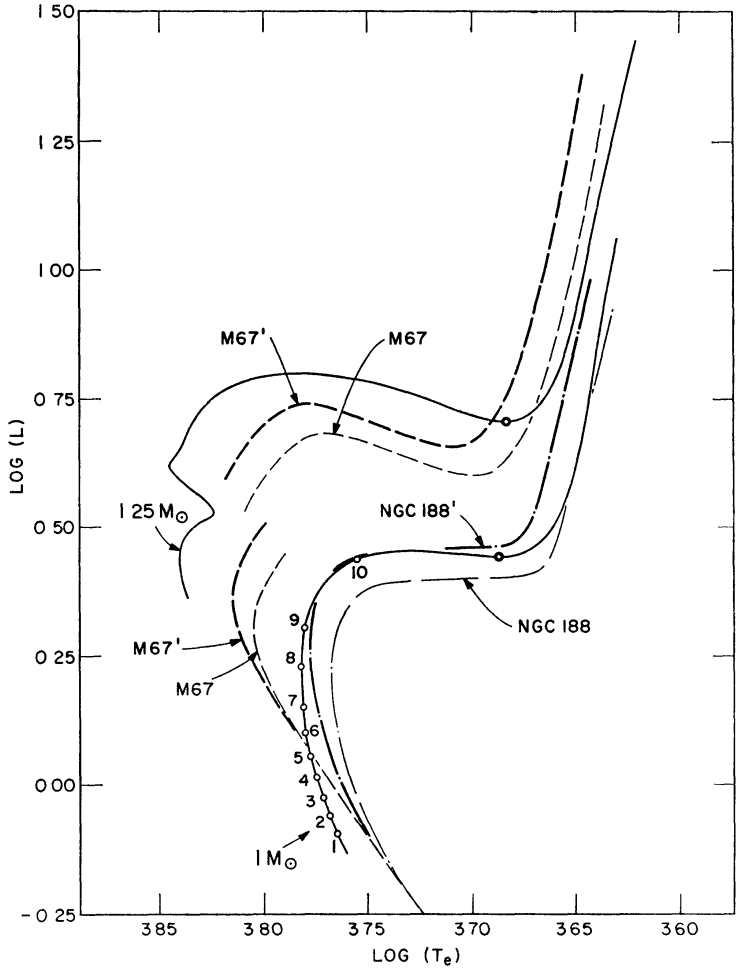


FIG. 25.—The comparison of M67 and NGC 188 with theoretical tracks in the log $L$, log $T_e$ plane. The mass appropriate to individual tracks is placed beside each track. The number corresponding to each circled point along the 1 $M_\odot$ track gives the time in $10^9$ yr required by a 1 $M_\odot$ star to reach that point from time of formation. The curves M67 and NGC 188 are identical in form with the curves in Fig. 24, but have been shifted bodily to higher surface temperatures by $\Delta(\log T_e) = 0.0175$. The curves M67′ and NGC 188′ have been shifted by $\Delta(\log T_e) = 0.0275$.

An age estimate may now be accomplished simply, without the construction of detailed time-constant loci. This estimate rests on the observation that, since the evolution of individual stars is extremely rapid during and following the shell-narrowing phase, the subgiant and giant portions of a cluster will look very much like the subgiant and giant portions of individual tracks corresponding to the most massive stars present in the cluster. In particular, a rough value of the cluster age may be assigned by determining the time required by an individual star to reach the relative minimum in luminosity at the base of the cluster red-giant branch. That is, the luminosity at the base of the cluster giant branch will coincide roughly with the luminosity at the base of the giant branch of an appropriately chosen star. The unnumbered circles along the 1 $M_\odot$ and 1.25 $M_\odot$ tracks in Figure 25 define the relevant base for these stars.

By means of the log $L$ versus $t$ curves in Figures 2, 4, and 6, the time for a star to reach the base of its giant branch (points 10 in Fig. 1) may be related to the luminosity at the base. The resulting relation may be expressed to the stated accuracy by

$$\log t \text{ (years)} = 10.00 - 1.50 \, [\log (L/L_\odot) - 0.45] \, .$$

For the two choices of cluster placement in Figure 25 one then obtains (1) $\tau_{\text{NGC 188}} \cong 9.8 \times 10^9$ yr; $\tau_{\text{M67}} \cong 4.9 \times 10^9$ yr; and (2) $\tau_{\text{NGC 188}} \cong 12 \times 10^9$ yr; $\tau_{\text{M67}} \cong 6 \times 10^9$ yr. Averaging these results gives the final values (3)

$$\tau_{\text{NGC 188}} = (11 \pm 2) \times 10^9 \text{ yr} \, ,$$

$$\tau_{\text{M67}} = (5.5 \pm 1) \times 10^9 \text{ yr} \, .$$

As a check on consistency, note that the cluster curves for M67 cross the 1 $M_\odot$ evolutionary track at about $5.5 \times 10^9$ yr.

It is a pleasure to thank (1) George Herbig for supplying the motivation to discuss lithium depletion and (2) W. A. Fowler for supplying the motivation to emphasize the production of $He^3$ in stars. Thanks are due to the Laboratory for Nuclear Science at the Massachusetts Institute of Technology for the use of its IBM 7044 computer and to the California Institute of Technology for the use of its IBM 7094 computer. The Center for Space Research at the Massachusetts Institute of Technology has been most generous in supplying financial support.

## REFERENCES

Arp, H. C. 1958, *Hdb. d. Phys.* (Berlin: Springer-Verlag), **51**, 75.
Demarque, P. R., and Larson, R. B. 1964, *Ap. J.*, **140**, 544.
Faulkner, J. 1966, *Ap J.*, **144**, 978.
Faulkner, J., and Iben, I., Jr. 1966, *Ap J.*, **144**, 995.
Fowler, W. A , Hoyle, F., and Wagoner, R. 1966, private communication.
Hayashi, C., Hōshi, R., and Sugimoto, D. 1962, *Progr. Theor. Phys. Suppl* , No 22.
Hofmeister, E., Kippenhahn, R., and Weigert, A. 1964, *Z. f. Ap.*, **6**, 57.
Iben, I., Jr. 1963, *Ap. J.*, **138**, 452.
———. 1965*a*, *ibid.*, **141**, 993 (Paper I).
———. 1965*b*, *ibid.*, **142**, 1447 (Paper II).
———. 1966*a*, *ibid.*, **143**, 483 (Paper III).
———. 1966*b*, *ibid.*, p 505 (Paper IV).
———. 1966*c*, *ibid.*, p. 516 (Paper V).
Johnson, H. L., and Sandage, A 1955, *Ap J.*, **121**, 616
Sandage, A. 1962, *Ap. J.*, **135**, 333.
Schönberg, M., and Chandrasekhar, S. 1942, *Ap J.*, **96**, 161.